THE APPLICABILITY OF GAMMA-RAY SPECTROMETRY WITHIN SOIL SCIENCE

A Thesis

by

GREGORY SCOTT ROUZE

Submitted to the Office of Graduate and Professional Studies of
Texas A&M University
in partial fulfillment of the requirements for the degree of

MASTER OF SCIENCE

Chair of Committee,	Cristine L.S. Morgan
Committee Members,	Haly L. Neely
	John A. Thomasson
Head of Department,	David Baltensperger

December 2015

Major Subject: Soil Science

ABSTRACT

Detailed spatial soil information is needed to better address environmental challenges across regional, national, and global scales. In the U.S., point-scale soil data are available to provide information on chemical and physical properties of soil as well as polygons where soils occur on the landscape. However, the soil data suffer from several shortcomings in terms of internal consistency as well as an inaccurate portrayal of soil variability. Passive aerial gamma-ray radiometrics is a tool that has been successfully used to represent soil variation because it may represent changes in parent materials. Legacy aerial gamma radiometric data is currently available across the United States but as such, has not been compared with soil properties. Therefore, the overall objective of this study was to assess the applicability of aerial gamma-ray spectrometry for the application of mapping soil properties associated across the U.S. Gamma radiometrics were compared with legacy soil samples across the United States. The quality of the initial aerial gamma-ray surveys were assessed by first comparing soil properties against with proximal gamma-ray surveys, followed by proximal and aerial radiometric comparisons within different parent materials in the state of Texas.

After determining that aerial gamma radiometric variation is best understood in terms of physiography, results indicated weak to moderately significant relationships between the two datasets for soil properties such as soil texture and cation-exchange capacity. Results support the conclusion that the soil sampling locations as well as the poor spatial resolution of the legacy gridded gamma radiometric data contribute to low

correlation coefficients. Proximal survey results indicate that aerial gamma-ray spatial patterns are related with soil properties such as texture and inorganic carbon within different parent materials. Results also indicate that poor geo-spatial positioning of aerial surveys drives the decrease in quality of correlations with soil data on the ground. Aerial gamma-ray spectrometry has utility for mapping soil properties, but consideration must first be given toward parent material and physiography type. Future studies should consider understanding aerial gamma radiometrics in the United States by surveying additional parent materials not present in this study.

ACKNOWLEDGEMENTS

Several years have passed, and while I still have a lot yet to learn, thanks to the following for helping me get started: Dr. Cristine Morgan, Dr. Haly Neely, Dr. T as well as Jason Ackerson. In terms of the work presented here, thanks to the undergraduate student workers for collecting lab data (Zach Prebeg, Jake Aitken, Brendan Olsen) and the field data from Alex Garcia, Jon Gross, Matt Bean and Julieta Collazo.

TABLE OF CONTENTS

LIST OF FIGURES

LIST OF TABLES

CHAPTER I

INTRODUCTION AND

LITERATURE REVIEW

Detailed spatial soils information for soil properties such as soil texture is needed for users interested in solving environmental problems such as proper land management as well as global soil security (McBratney et al., 2014). Soils information is typically presented either as qualitative (i.e. color, structure) or quantitative measurements (percent clay content), and individual soil series are differentiated from one another based on differences in these soil properties (McKenzie et al., 2008). In the early concepts of soil science, it was proposed by Jenny (1941) that different soils could be explained by under the five sources or factors of soil formation: climate, organisms, relief, parent materials and time (also referred to as the CLORPT model). When soils in the United States were first valued and assessed by governmental bodies such as the United States Department of Agriculture (USDA) in the 19th and 20th centuries, expert soil scientists differentiated between different soils by spatially delineating polygons or map units through experience as well employing the CLORPT model and historical remote sensing photography (Brevik et al., in press). Each soil map unit was then supplemented with soil data based on laboratory measurements and has since been managed and organized appropriately (McKenzie et al., 2008; National Cooperative Soil Survey, 2015). Although there are minor amounts of areas in the United States where

soils have not been mapped, the USDA has estimated that more than 95 percent of the all counties have been completed (Soil Survey Staff, 2015).

Although this type of legacy soil data is extensive on a national scale and contains mostly complete soil property information, it is not considered to be a reliable end-product for several reasons. First, the information provided within legacy soil maps may suggest to a user that soils vary discretely when in fact soils are known to vary continuously across a given landscape (Heuvelink and Webster, 2001). Potential problems with these maps are furtherly compounded because uncertainty is not characterized alongside soil property estimations and map quality assessment, therefore, is limited (McBratney et al., 2000). Second, legacy soil maps lack consistency because soil scientists employ their own conceptual models in describing soils, and often at different cartographic scales (Brevik et al., in press*).* Finally, these maps furtherly assume that estimates are static in nature, but many soil properties such as water content can exhibit high temporal variability (Brevik et al., in press). Therefore, there is a need to reliably represent soil variability such a way that is inherently free of bias (Hengl et al., 2014).

The need for spatially continuous soil information has since been formalized by McBratney et al. (2003) through the SCORPAN model, and, although the model is conceptually analogous with the CLORPT model, it suggests that soils can be described in terms of spatial location (n) according to Tobler's first law of geography (i.e. nearer soils are spatially correlated than those soils further apart) (Thompson et al., 2012). When the SCORPAN model was introduced by McBratney et al. (2003), soil scientists

began to look for tools that could be used to describe soils continuously and without bias, and once such answer has been found using soil sensor technology (Viscarra-Rossel et al., 2011). One example of a mobile soil sensor that has been used in the field of soil science is a passive gamma-ray spectrometer that measures gamma-rays passively emitted from the soil surface (Viscarra-Rossel et al., 2007).

I.1. Literature Review

I.1.1. Principles of Gamma-ray Spectrometry

Gamma-rays refer to massless, high energy particles located along the electromagnetic spectrum (between 10 to 10,000 keV) that form when initial radioelements (parents) release energy to form a different radioelement (daughters) in a random event called radioactive decay, and is expressed as:

$$N = N_0 e^{(\frac{-0.693t}{T_{1/2}})} \quad (1)$$

where N is the number of daughter atoms; N_0 is the number of parent atoms; t is the elapsed time; and $T_{1/2}$ is the half-life of a given radioelement (Gilmore, 2008). Gamma-ray particles contain an energy value based on the following equation:

$$E = h\nu \quad (2)$$

where E is the energy (in Joules or J); h is Planck's constant ($6.634*10^{-34}$ J s^{-1}); and ν is the frequency of the wavelength (s^{-1}). The value of ν can be expressed as

$$\nu = \frac{c}{\lambda} \quad (3)$$

where λ is the wavelength (in m), and c is the speed of light (m s^{-1}) (Minty, 1997b; IAEA, 2003). Energy values, which are originally expressed in Joules, can then be expressed in terms of electron volts when considering that 1 Joule = 6.24 x 10^{12} mega electron volts (MeV) (Gilmore, 2008). In GRS, each gamma-ray particle is detected by the sensor is summed over a given time period (usually one second), a value of which can explained by Beer's law

$$I = I_0 e^{(-\mu x)} \tag{4}$$

where I is the final intensity (in counts s^{-1}); I_0 is the initial radiation intensity (in counts s^{-1}); μ is the linear attenuation coefficient (or alternatively expressed as $\mu = \rho * \mu_m$, where ρ is the density of the soil and μ_w is the mass attenuation coefficient) and is proportional to the total number of electrons per unit volume of material; and x is the thickness of a given material (m^{-1}) (Beamish, 2014). The range in energy values that are typically given from gamma-ray spectra within a soil are 0.1 MeV to 3.0 MeV, with each detected gamma-ray energy sorted into different energy channels, a value of which depends on the detector in use.

I.1.2. Gamma-ray Interactions with Detectors and Instrumentation

Gamma-ray sensors have been developed to calculate the concentrations of natural radioelements from a gamma-ray spectrum based on three different interaction mechanisms of gamma-ray particles with matter (Darnley, 1991). First, a gamma-ray can transfer all of its energy into a valence electron of an atom at low energies - this is called the photoelectric effect. Second, an incoming gamma-ray can transfer a partial amount of energy towards a valence electron and undergo subsequent scattering, termed

Compton scattering. Compton scattering is the main form of interaction at the energies used in gamma-ray studies and is often seen in gamma-ray spectra at lower energies called the Compton continuum (Gilmore, 2008). Third, an incoming gamma-ray can be become fully absorbed, creating an electron-positron pair and subsequently annihilates into two gamma-ray photons of equal energy; this process is called pair production (Minty, 1997b; IAEA, 2003; Gilmore, 2008).

Different gamma-ray spectrometer types have been created that account for these interactions mechanisms using either a scintillator or a semiconductor. In a scintillation spectrometer, an incoming gamma-ray interacts with a scintillation crystal (typically NaI or CsI) to produce visible photons (i.e. scintillations) that cause electrons to be ejected at a photocathode, or a negatively charged electrode, and a negative voltage is created that is proportional to the original gamma-ray energy (IAEA, 2003). Scintillation spectrometers have been more widely used in environmental studies because they are relatively cheaper to manufacture than semiconductors, which allows for larger detector volumes (and therefore shorter measurement times); however, sensors that use scintillation crystals are subjected to a higher probability of performance failure because the manufactured crystals themselves are often fragile (Minty, 1997b).

Semiconductor gamma-ray spectrometers are an additional solid-state device that consist of a valence band, a conduction band, and an energy gap between two bands. When an incoming gamma-ray interacts with the semiconductor material, electrons that are bound to atoms become excited and move through the energy band to the conduction band, leaving a hole or vacancy that can become filled by other electrons within the

valence band; the electrons that are found in the conduction band from gamma-ray excitation de-excite and are moved by an applied electric field out of the detector, thereby allowing gamma-rays to be identified under the assumption that the number of electron-hole pairs created is proportional to the energy of the initial gamma-ray (Gilmore, 2008). Semiconductors are generally lower in volume and more expensive than scintillation crystals but can exhibit a higher energy resolution (Hendriks et al., 2001). Solid-state detectors are typically used for in-situ surveys or in the lab because the crystal requires constant cooling through liquid nitrogen in order to reduce the noise or background current of the system (Gilmore, 2008).

I.1.3. Sources of Gamma-ray Radiation within Soils

Radioelements occurring in soil are naturally occurring and include Potassium (^{40}K), Uranium (^{238}U) and Thorium (^{232}Th), and comprise 0.012, 0.72 and almost 100 percent of their respective natural occurring elements (Minty, 1997b; Gilmore, 2008). Cesium (^{137}Cs) is also found in soil and is formed through anthropogenic activities such as radioactive fallout from nuclear tests (Ritchie and McHenry, 1990). The peaks and energy windows that are typically used to estimate ^{40}K, ^{238}U and ^{232}Th concentrations are provided in Table 1.

Gamma-rays are directly released in the decay of ^{40}K to ^{40}Ar, while ^{232}Th and ^{238}U are emitted from daughter products further down their respective decay chains. ^{232}Th and ^{238}U are thus more susceptible to disequilibrium, a condition where the rate of product formation does not equal the rate of parent decay (Minty, 1997b). For example, the daughter products of ^{238}U are ^{222}Rn and ^{214}Bi can be lost or leached from the soil

system in heavy rainfall or oxidizing conditions, leading to a decrease in the signal to noise ratio for estimates of ^{238}U (Minty, 1997b). Although ^{238}U and ^{232}Th are found in smaller concentrations than ^{40}K within soils, ^{238}U and ^{232}Th are more likely to be retained on clay surfaces when weathering begins to take place, whereas ^{40}K is more easily weathered out of silicate clays and subsequently leached (Wilford et al., 1997).

Table 1: Radioelements that are commonly analyzed within gamma-ray spectrometry.

Radioelement	Gamma-Emitting Product	Half-life (years)	Peak Energy (MeV)	Standardized Energy Window (MeV)
Potassium (^{40}K)	^{40}K ($^{40}K \rightarrow {}^{40}Ar$)	$1.3x10^{9}$	1.46	1.370-1.570
Uranium (^{238}U)	^{214}Bi	$4.46x10^{9}$	1.76	1.660-1.860
Thorium (^{232}Th)	^{208}Tl	$1.39x10^{10}$	2.61	2.410-2.810
Cesium (^{137}Cs)	^{137}Cs	30.12	0.662	0.562-0.762

I.1.4. Gamma Radiometric Collection Methods

Regardless of whether the gamma-emitting source is natural or anthropogenic, sensor technology or gamma-ray spectrometers are able to register and differentiate between different gamma-ray energy values quite efficiently (Darnley, 1991). Gamma-rays are able to be registered by the sensor because they interact with the hardware to produce scintillations of light or electricity that are subsequently converted into digital signals (Gilmore, 2008).

The initial use of these sensors within a soil science framework was for laboratory purposes, but has since shifted towards the field. Gamma-ray field surveys can take place either in the air (aerial gamma radiometrics) or closer to the ground (proximal gamma radiometrics), the latter of which can be sub-characterized into portable-traversed (either on foot or stationary) or vehicle-traversed surveys (IAEA, 2003; Kock and Samuelsson, 2011). Aerial gamma radiometrics provides the largest sampling coverage because these sensors are equipped onto helicopter or fixed-wing aircraft and are not bound by obstacles such as fence lines, although navigation clearance can be a concern, especially over urban areas (Cresswell et al., 2013; Stockmann et al., 2015).

Portable-traversed and vehicle-traversed GRS surveys in contrast with aerial gamma radiometrics surveys sample less area and typically use a smaller amount of crystal volume in the case of scintillation spectrometers. The appropriate choice of survey method (ground versus aerial) can be understood only when the intended use of the gamma-ray data is clearly defined and resources in terms of time and money are known (Killeen, 1979). In contrast with portable-traversed gamma-ray surveys, vehicle-borne surveys are more efficient in characterizing soil processes within multiple landscapes due to its relatively larger sampling coverage, and recent literature has suggested that vehicle-traversed surveys can be considered to be an alternative to aerial surveys if a 'smart' ground survey is undertaken (Stockmann et al., 2015).

I.1.5. Gamma-ray Data Processing and Post-processing

Once a raw gamma-ray spectrum is obtained, it is then corrected for background radiation (i.e. sources of gamma radiation not emitted from the soil), and are

subsequently converted into mass concentration values (i.e. % ^{40}K, ppm soil ^{238}U and ^{232}Th) within the soil through the following steps: 1) live-time correction; 2) energy calibration; 3) vehicle and cosmic correction; 4) radon background correction; 5) channel interaction or stripping correction; 6) height correction and final conversion into concentration based on derived calibration constants (Minty, 1997b; IAEA, 2003).

Note that some of the processing steps listed above are more relevant than others depending on the type of gamma-ray survey conducted (ground/proximal versus aerial survey). For example, aerial gamma-ray surveys require more background correction in the form of cosmic and radon than ground surveys because the detector encounters more of these types of particles (IAEA, 2003).

Unfortunately, gamma-ray spectra that are collected in aerial surveys are usually subjected to environmental effects that attenuate the gamma-ray flux, such as excessive soil moisture from a previous rainfall, snow cover, or vegetation (IAEA, 2003). Soil moisture operates as an effective gamma-ray attenuating material because water contains hydrogen ions which act to provide additional electron content, thereby allowing for more possible gamma-ray and electron interactions (Løvborg, 1984). Therefore, gamma radiation measurements can be modified for soil moisture using the following equation:

$$N_w = N_d \frac{1}{1 + k\theta_w} \tag{5}$$

where N_w is the measured intensity of gamma radiation; N_d is the intensity of gamma radiation when the soil is dry; k is the ratio of electrons in water to that of soil (k = 1.11); and θ_w is gravimetric soil water content (Loijens, 1980; Carroll, 1981).

Additionally, post-processing methods have been applied to reduce the overall effect of noise, such as spectral component analysis (Hovgaard and Grasty, 1997) and spatial and therefore temporal averaging using neighborhoods (Rawlins et al., 2012; Viscarra-Rossel et al., 2014).

I.1.6. History of Gamma-ray Spectrometry within the United States

In the United States, the first aerial gamma radiometrics surveys began in 1973 through the United States Geological Survey (USGS) due to an interest in characterizing uranium resources, under the hypothesis that rocks contain different aerial gamma responses in uranium (Hill et al., 2009). For example, sedimentary rocks generally emit high amounts of uranium because they contain uranium rich minerals such as zircon, xenotime and monazite, although such concentrations are typically higher in igneous rocks (Killeen, 1979). The previous generalizations applied to uranium do not, however, indicate that a classification system can be created based on the gamma signals because it is quite common that different parent materials emit similar amounts of gamma-ray energies (Killeen, 1979).

Legacy aerial surveys conducted by geological agencies such as the USGS initially collect raw counts but are then post-processed to obtain mass concentration values using the steps outline in section 2.5. To provide gamma-ray measurements between individual transect lines across the entire U.S., all of the points were interpolated onto relatively coarse grids (i.e. cell resolution of 2 kilometers), and broad regional trends can be observed in terms of the gamma variable called dose rate (Fig. 1) (IAEA, 2003; Duval, 2005). Dose rate has been defined by IAEA (2003) as the amount of energy imparted

onto a unit of matter per unit time (nanoGrays hr^{-1}), and is calculated in the following equation:

$$Dose\,Rate = 13.2*[K] + 5.48*[U] + 2.72*[Th] \quad (6)$$

where K is the concentration of ^{40}K in percent; U is the concentration of ^{238}eU in ppm and ^{232}eTh is the concentration of ^{232}Th in ppm under equilibrium ('e') conditions. In Fig. 1, high dose rate values can be seen in the western United States, in particular the state of Nevada, which contains pyroclastic rhyolitic (fine-grained acidic rock with enriched potassium) tuff parent materials that were ejected from volcanoes between the Miocene and Oligocene time periods (Best et al., 1989). Low amounts of gamma radiation in Fig. 1 can also be seen along the Florida coast and can be explained through the presence of peat deposits, which are known to store high amounts of water, thereby attenuating significant amounts of gamma-rays (Beamish, 2014).

I.2. Application of Aerial Gamma-ray Spectrometry to Soil Science

Soon after connections were made between aerial gamma radiometrics and geology, research scientists soon began to realize the potential benefits of aerial gamma radiometrics within soil science because soils inherit characteristics from its underlying weathered bedrock, or parent material (Wilford et al., 1997). These researchers then hypothesized (and confirmed) that, if lithology can be distinguished based on the aerial gamma radiometrics signal at regional scales, then soils could be differentiated as well because they inherit mineralogy from their underlying parent materials (Schwarzer and Adams, 1973; Darnley, 1991; IAEA, 2003). This assumption may not hold true,

however, for soils that form over multiple parent materials lithological discontinuities (Dickson and Scott, 1997).

Once this relationship between soil science and aerial gamma radiometrics was established (Schwarzer et al., 1971; Schwarzer and Adams, 1973), researchers began investigating just how well aerial gamma-ray data can be used to predict spatially variable surface soil properties derived from parent materials such as soil texture (Taylor et al., 2002). Clay content and cation-exchange capacity (CEC) have been considered the primary soil attributes that can be mapped using aerial gamma radiometrics because these two collinear variables are generally associated with silicate clay mineralogy (Wilford and Minty, 2007). For example, it has been generalized within literature that higher amounts of gamma-ray emitting radioelements such as uranium and thorium are found on the surface area of soil constituents found within clay minerals (Megumi and Mamuro, 1977). This assumption may not always hold true, however, for soils can contain clay sized particles that are not significant emitters of gamma radiation, such as calcium carbonate, for example ($CaCO_3$), thereby interfering with the relationship provided by clay content (Stockmann et al., 2015). Note that the type of clay mineral found within soils will affect the CEC, and thus its collinearity with clay content.

In contrast to clay content and CEC, secondary soil properties such as sand content, pH and calcium carbonate ($CaCO_3$) have been related with GRS data, but not with aerial gamma radiometrics data (Viscarra-Rossel et al., 2007; Priori et al., 2013). Sand content would be expected to have an inverse relationship with GRS because sand particles consist of minerals that are poor emitters of gamma-ray radiation such as quartz that are

highly resistant to chemical and physical weathering conditions, and such relationships are mirrored with that of clay content (Wilford, 1997, Mahmood et al., 2013). Although pH is similar to texture and CEC in that it is influenced by parent material type, these two properties have potential to have stronger relationships with aerial gamma radiometrics because such variation is less affected by management practices (Bierwirth, 1996). Soils derived from parent materials with large concentrations of $CaCO_3$ generally emit low amounts of gamma radiation, and has been negatively correlated with aerial gamma radiometrics due to associations with silica-rich dune fields or a dilution effect in ^{40}K-rich soils (Pickup and Marks, 2000; Wilford et al., 2015).

The relationships between aerial gamma radiometrics and primary and secondary soil properties are not stable and can be altered based on topographic attributes, such as slope and relief (Wilford, 2012; Viscarra-Rossel et al., 2014). These terrain variables are often related with gamma-ray spectrometry because erosional forces (i.e. high slopes) can cause radioelements to be physically transported across a landscape (Wilford and Minty, 2006). In consideration of optimal parent materials and physiographic types, it was hypothesized by Rawlins et al. (2007) that aerial gamma radiometrics has the most utility within young, unconsolidated sediments located in flat areas because gamma-ray emitting soil materials will not be lost due to insufficient physical and chemical weathering rates. However, the study conducted by Rawlins et al. (2007) only considered landscapes that formed from eastern England, and not those from the United States. Hence, there is an additional need to address the effect of topography or physical geographic type (physiography) on the relationship between and aerial gamma

radiometrics and soils databases within the United States because such knowledge is currently lacking.

It is important to gain an understanding of how parent material and physiographic types affect the relationship between aerial gamma radiometrics and soil properties, and such knowledge is necessary in assessing the usefulness of legacy aerial gamma datasets because only then can its predictive power of soil properties be known, especially when compared with that of environmental covariates (McBratney et al., 2003). The purpose of environmental covariates (such as gamma-ray imagery, Fig. 1) are to generate accurate predictions of spatial soil properties through pedometric techniques such as regression-kriging (McBratney et al., 2000; McKenzie et al., 2008). Several papers (McKenzie and Ryan, 1999; Levi and Rasmussen et al., 2014) underwent comparative analysis of several environmental covariates to predict spatial soil properties, such as Landsat images and solar radiation, but as of yet aerial gamma radiometrics has not been implemented in such studies nor compared with these covariates (Rawlins et al., 2007).

If the primary goal is to use gamma radiometric data to understand spatial soil variation across national scales, there is a need to establish a more fundamental relationship between the two datasets rather than through correlation analysis because the two datasets operate at different spatial scales and thus the relationships drawn with soil properties questionable (Kock and Samuelsson, 2011).

One method of validating an aerial signal is to conduct ground surveys because the latter operates under more similar support volumes (Cardarelli II et al., 2011). Although the method is more expensive than analyzing pre-existing aerial gamma radiometric

datasets, proximal gamma-ray sensors (grouped by portable- or vehicle- traversed) are often preferred over aerial gamma-rays sensors where higher resolution soil data is needed in the case of relatively large line spacing distances for aerial surveys (Viscarra-Rossel et al., 2007).

The purpose of the proximal gamma-ray surveys is to form a baseline that suggests what aerial raw gamma *should* be responding to in terms of its relationship with soil properties because the former collects data at a relatively higher signal-to-noise ratio and thus functions as a form of ground-truthing for raw aerial gamma-ray surveys (Bollhöfer et al., 2013). Proximal surveys measure naturally emitted gamma-rays from a smaller area than aerial sensors, thereby allowing for more accurate estimates at a given point location than aerial sensors because proximal sensors operate on a scale more similar to that of soil variability.

Ground-truthing overall involves establishing a relationship between the response that is expected (proximal) with the response that is provided (aerial), and is necessary to validate the response given from aerial gamma radiometrics (Bollhöfer et al., 2013), and initial analysis of ground-truthing within literature suggests that it is most successful when aerial gamma radiometric data is variable itself. For example, Kock and Samuelsson (2011) compared aerial and backpack gamma measurements (i.e. ^{40}K, ^{238}U and ^{232}Th) for three different parent materials in southern Sweden, and found that ^{238}U and ^{232}Th contained the highest regression correlation coefficient (R^2) because there was at least one site within each radioelement that was much more variable than the rest. In their study, portable-traversed proximal gamma surveys were conducted. Note that the

analysis conducted by Kock and Samuelsson (2011) does not consider a vehicular gamma-ray analysis, whereby a larger spatial coverage is offset by a potentially higher source of noise compared with portable-surveys primarily because the latter is able to control the sampling time (and thus lower uncertainty).

I.3. Study Aims

The overall goal of this research is to evaluate the reliability of aerial gamma-ray spectrometry in characterizing soil properties. Specifically, this research addresses the following objectives: 1) identify the usefulness of legacy USDA-NRCS soil property data in explaining aerial gamma radiometric data across the United States; 2) quantify the utility of pre-existing aerial gamma radiometric data in predicting selected soil properties (e.g. clay, sand, CEC, CaCO3, pH) within both parent material and physiographic types; 3) assess the usefulness of pre-existing aerial gamma radiometric data in comparison with other environmental covariates through predictions of clay content within a given environmental setting; 4) identify relationships between soil properties and gamma-ray spectra using a vehicle-borne gamma-ray spectrometer across different landscapes; and 5) validate aerial gamma-ray spatial patterns with proximal gamma-ray surveys across different landscapes.

CHAPTER II

EXPLORATORY ASSESSMENT OF UNITED STATES AERIAL GAMMA RADIOMETRICS

II.1. Introduction

Accurate and up-to-date digital soil data is needed for solving global environmental challenges such as food, water and energy security decisions at regional, continental and global spatial scales. Digital soil maps, at appropriate spatial resolutions, can help address the need to quantify soil capability and locate soils with specific functionalities (Koch et al., 2013). In the United States, soil information is prevalent and has been made available online by the United States Department of Agriculture National Resources Conservation Service (USDA-NRCS) in the form of historical or legacy soil polygon maps. Delineations made by surveyors would either be confirmed or altered after collecting and analyzing geo-referenced soil samples for physical and chemical soil properties in the laboratory (Soil Survey Division Staff, 1993). Each of the geo-referenced, lab characterized, samples were then stored and managed within an publicly available digital database called the National Cooperative Soil Survey Characterization Database (NCSS-SCD) (National Cooperative Soil Survey, 2015). Through these historical soil survey programs, it has been estimated that up to 95 percent of all land in the United States has been delineated using the soil polygon approach (Brevik et al., in press).

Although legacy soil datasets are quite extensive and are easily accessible, they are not considered to be the ultimate end-product for assessing soil capacity across the conterminous U.S. for several reasons. First, historical or legacy data suggest that soils vary discretely, but soils actually vary continuously, resulting in maps that contain fuzziness or uncertainty (Heuvelink and Webster, 2001). Second, legacy soil maps lack consistency because soil scientists described soils based on their own personal experiences and local traditions, and such mapping exercises often occurred at different cartographic scales (Brevik et al., in press). Therefore, there is a need to reliably represent soil spatial variability in such a way that is accurate, continuous, and consistent in such a way that removes personal bias (Hengl et al., 2014).

Sensor technology that provides objective, and spatially continuous information has been proposed as an alternative solution to direct soil sampling methods. One advantage to using sensor measurements is that sensor data are continuous in geographical space, under the assumption that such data functions as a surrogate for a soil forming process or factor (Viscarra-Rossel et al., 2011). Another advantage gained by using sensor technology over pre-existing soil mapping methods is that it can have a lower amount of bias because measurements are physically based and are therefore limited in subjectivity (Hartemink and Minasny, 2014). The use of sensor technology is not new within the field of soil science, as electromagnetic induction, GPR, visible and near infrared spectroscopy, among other proximal and remote sensors have been used at the field (m) scale to understand spatial soil patterns of soil variability (Annan, 2002; Adamchuk et al., 2004; Stenberg et al., 2010; Doolittle and Brevik, 2014).

An example of a sensor that has recently been used to map spatial soil variation of physical and chemical properties is a passive gamma-ray spectrometer. This type of spectroscopy detects and measures very high frequency electromagnetic radiation that is passively emitted from soil minerals due to radioactive decay of radioelements such as ^{40}K, ^{238}U and ^{232}Th (Wilford and Minty, 2006; Gilmore, 2008). Under the assumption that the spatial distributions of ^{40}K, ^{238}U and ^{232}Th are indicative of changes in soil parent materials, aerial gamma radiometrics have been used to map soils and their weathering intensities at high altitudes (20 to 120 m) and coarse line-spacing distances (0.4 to 10 km) in Australia. The association of aerial gamma radiometrics with soil and geology has also been used to map peat thicknesses within the United Kingdom, based on the attenuation of gamma-rays by peat and water in peat (Beamish, 2015). But such investigations are currently lacking within the U.S., although aerial gamma radiometrics data is currently available across the entire nation (Cook et al., 1996). Additionally, aerial gamma radiometrics have not been quantified in terms of relationships with measureable soil properties, which are relevant to addressing soil capability and quality (Arrouays et al., 2014).

Initial investigations into relationships between aerial gamma radiometrics and soil properties have indicated that gamma radiometrics are most useful in mapping soil properties associated with soil mineralogy. For example, soil texture has been associated with gamma radiometrics because most clay-sized particles (i.e. less than 2.0 μm) are associated with silicate clays, and these minerals comprise of radioactive elements that emit gamma-rays under radioactive decay (Schwarzer and Adams, 1973; Rawlins et al.,

2007; Gilmore, 2008). In addition to soil texture, cation-exchange capacity (CEC), and to a lesser extent pH and calcium carbonate equivalent (CCE) have also been linked with gamma radiometric data (Viscarra-Rossel et al., 2007; Priori et al., 2013; Priori et al., 2014). These results, however, have only been understood through the use of high resolution proximal gamma radiometrics which, unlike aerial gamma radiometrics are spatially limited to single or few amounts of parent materials.

Before soils and their properties (clay and sand contents, CEC, CCE and pH) can be linked with proximal gamma radiometric data, it is necessary to first identify sources that contribute to an aerial gamma radiometric signal, and determine if one of these sources can be attributed to soil mineralogy. An initial study in linking aerial gamma radiometrics signals with soil geochemistry has been conducted by Rawlins et al. (2007), whereby aerial ^{40}K and ^{232}Th estimates were compared with soil ^{40}K and ^{232}Th geochemical measurements through simple correlations. In their results, they found strong agreement across relatively small spatial scales (1:50,000) in eastern England. England has more youthful landscapes and less weathered soils compared to the US. In addition, the methodology of Rawlins et al. (2007) did not include comparisons between aerial gamma radiometrics and other standardized indicators of clay mineralogy such as clay content and CEC.

If soil properties such as clay content could be mapped with aerial gamma radiometric data, it would then become beneficial to establish where it is most useful-geographically. For example, Bierwirth (1996) suggested that ^{40}K and ^{232}Th can be used to map textural variation within youthful alluvial deposits because these radioelements

are in relatively high abundances. In contrast, mountainous areas that exhibit erosional rates are less likely to map variations in clay content because the aerial gamma radiometric signal is more indicative of bedrock composition rather than clay mineralogy (Bierwirth, 1996). Thus, the geomorphic or physiographic setting of a given location can affect relationships between aerial gamma radiometrics and soil properties.

The importance of assessing soil capability in terms of quantifiable soil properties using aerial gamma radiometrics has practical relevance within the Digital Soil Mapping community. Current soil maps that adhere to the GlobalSoilMap standards should have a 1 km resolution which requires spatial predictive functions for soil properties that incorporate covariates representing soil forming factors such as climate and topography (Arrouays, et al., 2014; Hengl et al., 2014). Most soil predictive models are not including covariates that represent parent material, especially representation of parent material information that is independent of topography indices. Aerial gamma radiometric data provides a source of information that can represent parent materials. To exploit this potential data source it would be useful to know how well it represents parent material and how well aerial gamma radiometrics relates to soil properties—particularly in the conterminous U.S.

The overall goal of this work is to identify the usefulness of aerial gamma radiometric data for soil mapping within and between different landforms and landscapes of the United States. The first specific objective is to evaluate the variability in aerial gamma radiometric data across the United States through a fixed-effect or regression model analysis that uses soil clay content (continuous), parent material

(categorical) and physical geography or physiography (categorical) types as fixed effects or predictor variables. The second objective is to quantify the utility of pre-existing aerial gamma radiometric data in predicting selected soil properties (e.g. clay and sand contents, CEC, pH and CCE). The third objective is to evaluate the utility of aerial gamma radiometric data as a covariate for parent material for spatial predictions of soil clay content.

II.2. Materials and Methods

II.2.1. Data Sources

Legacy soil data was obtained from the NCSS Soil Characterization Database (NCSS-SCD), and the surface horizons were selected, based on the assumption that emitted gamma-rays are located primarily from the surface (IAEA, 2003; National Cooperative Soil Survey, 2015). In total, 44,152 geo-referenced surface samples across the United States were selected, and the geographical coordinate system for the NCSS-SCD was set to North American Datum 1983 (Schoeneberger et al, 2012). Soil properties that were chosen in this study include 1) clay and sand content (either pipette or hydrometer methods), 2) cation-exchange capacity (NH_4-Ac method), 3) pH ($CaCl_2$ method) and 4) calcium carbonate equivalent (CCE) (3 N HCl method) (Soil Survey Staff, 2014).

The aerial gamma radiometric datasets used for this study include dose rate, or radiation energy imparted onto a unit soil of mass per unit time (nGy hr^{-1}), potassium (^{40}K), uranium (^{238}eU), and thorium (^{232}eTh) (IAEA, 2003; Duval et al., 2005; Hill et al., 2009) (Equation 6 and Fig. 1). The projected coordinate system for the aerial gamma

radiometric raster maps is Conic Albers Equal Area, USGS Version, with a cell resolution of 2 km.

To account for the effect of physiography on aerial gamma radiometric data, the surface soil samples were separated into areas of regional similarity based on a digitized physiographic map created by Fenneman (1917) which divides individual areas based on differences in landforms and other confounding effects such as climate and vegetation. In total, there are eight different physiographic divisions (broadest scale delineations), 25 provinces, and 77 sections (finest scale delineations) across the United States, and the division grouping was used here in order to simplify results across the conterminous United States (Fig 2.). The Laurentian Uplands, Atlantic and Interior Plains are characterized by flat topography, while the Appalachian and Interior Highlands, and Rocky and Pacific Mountain Systems are characterized by mountain ranges (Fig. 2). The coordinate system for the physiographic map is Albers Equal Conic Area, USGS Version.

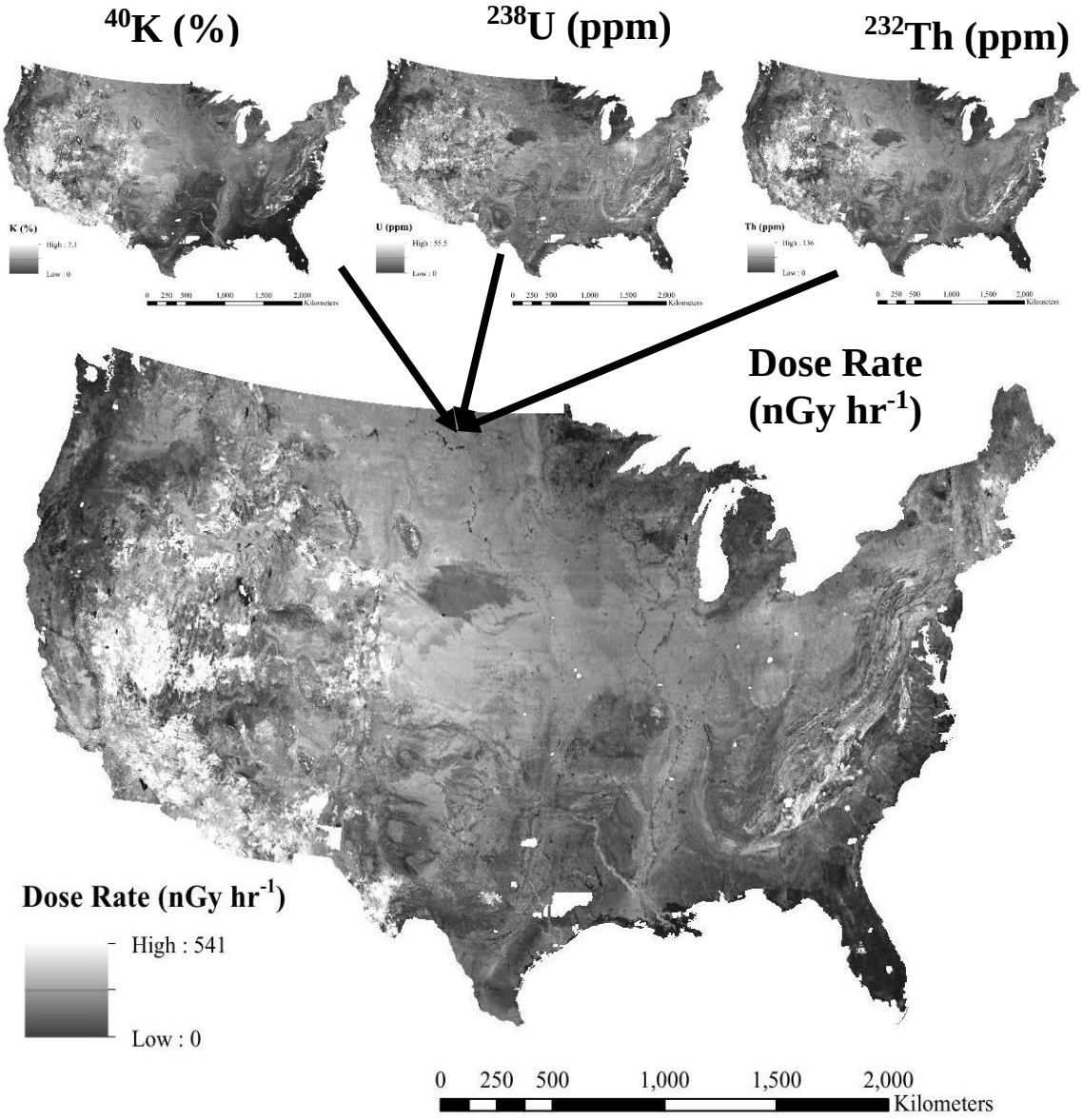

Figure 1: Interpolated aerial gamma radiometric maps of ^{40}K, ^{238}U, ^{232}Th, and dose rate across the conterminous United States as provided by the United States Geological Survey (USGS). Reprinted from Duval et al. (2005).

In addition to physiography, a surficial parent material map (scale 1:5,000,000) was obtained from the USGS and used in the analysis to represent parent materials for soils within the NCSS-SCD database (Soller et al., 2009) (Figure 3). Due to the large amount of detailed parent material types represented within the database (51), the map was reclassified into 15 broader parent material types to simplify the analyses across the United States (Fig. 3). The United States is characterized by parent materials such as glacial (i.e. glacial till and glaciofluvial) deposits in the northern states, igneous, metamorphic and carbonate-rich residuum in the western states, and unconsolidated sediments such as alluvium and coastal deposits adjacent to the Gulf of Mexico (Fig. 3).

Additional digital covariates such as the gridded Soil Survey Geographic (gSSURGO) or rasterized soil polygon map and Shuttle Radar Topography Mission Digital Elevation Model data for relief and slope were assembled along with aerial gamma radiometric data to predict clay content in three different soil landscapes based on results obtained from objective 2 (Jarvis et al., 2008; Soil Survey Staff, 2015a). The non-aerial gamma radiometric environmental covariates were selected to represent different components of the well-known SCORPAN model such as: 1) clay content from gSSURGO database, 2) elevation, and 3) slope (McBratney et al., 2003). Lithology was not selected because the Southern High Plains was mostly uniform and the aerial gamma radiometrics is expected to represent lithology, or parent material to some degree. Covariates were not considered for the *c* and *o* components of the scorpan model due to differences in temporal resolutions.

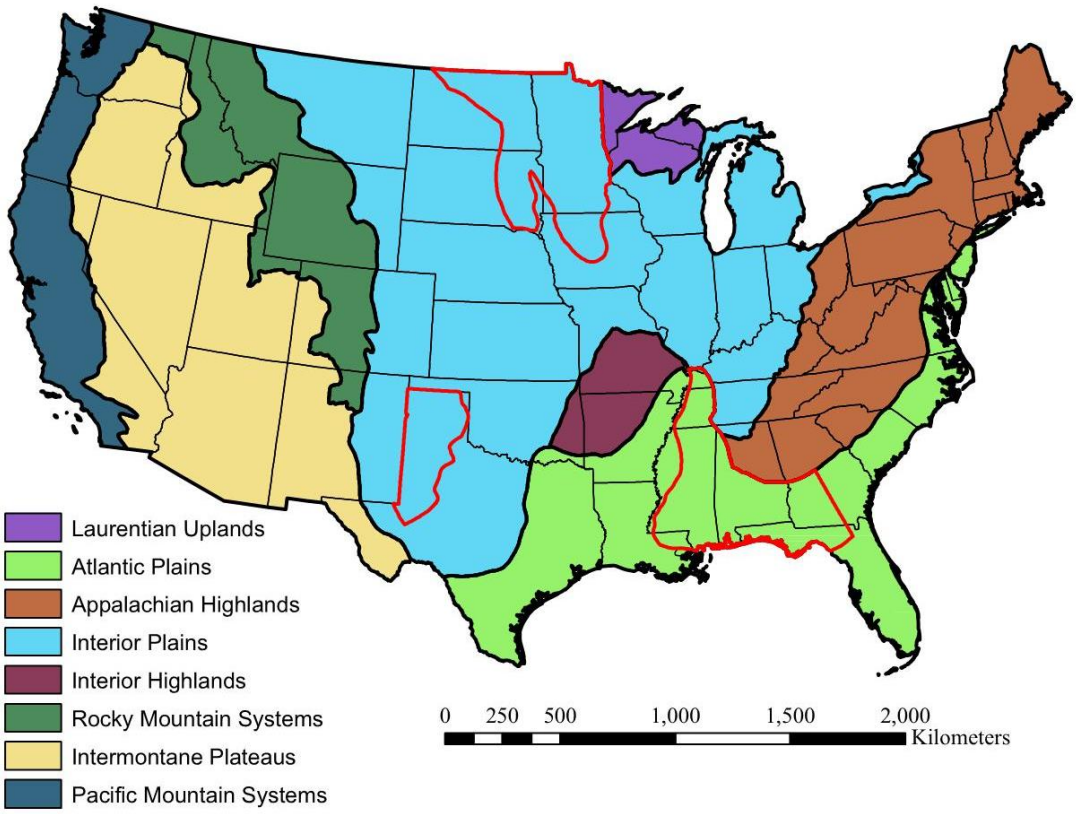

Figure 2: A physical geographic (physiographic) map across the conterminous United States. Reprinted from Fenneman (1917).The black delineations refer to the broadest delineations of physiography called divisions, while the selected polygons (red) within each of the divisions are the finest delineations termed sections that represented areas that were analyzed in objective 3 based on suitability classifications for clay content (refer to text).

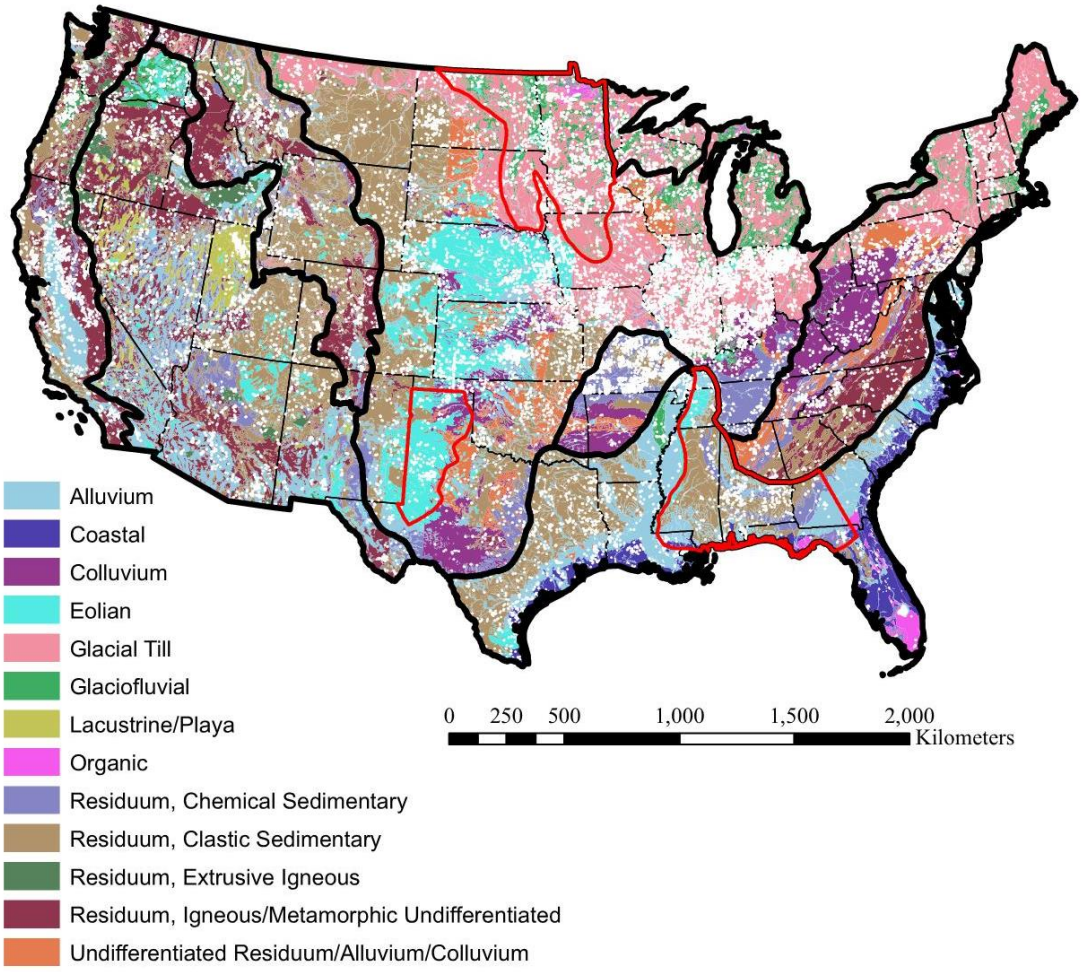

Figure 3: A reclassified surficial parent material map across the conterminous United States. Reprinted from Soller et al. (2009). Soil samples from the NCSS-SCD are outlined by white points and separated into different physiographic divisions (black) and sections (red) as shown in Figure 2.

Soils from the NCSS-SCD were spatially joined with the physiography, parent material and gamma radiometric maps and subsequently imported into the R statistical software program (R Development Core Team, 2014). Soil samples that were not geo-referenced or contained negative aerial gamma radiometric measurements were removed (n = 40,418). Soil properties of multiple soil samples that lie within the same 2-km grid cell were then averaged (n = 22,536). Gamma and soil properties were subsequently transformed using methodology described by Sheather (2009) to achieve data normality, and summary statistics of soil and gamma properties are shown in Table 2.

Table 2. Descriptive statistics of soil properties from the National Cooperative Soil Survey Characterization Database after removing multiple samples (n = 22,536).

Soil Property†	**Units**	**Range**	**Std. Dev.**	**Mean**	**CV**
Clay	g kg^{-1}	0 - 91	12	19	0.63
Sand	g kg^{-1}	0 - 100	26	36	0.72
CEC	$cmol_+$ kg^{-1}	0 - 206	17	20	0.85
pH	mol L^{-1}	2.4 - 10.4	1.2	5.8	0.21
CCE	%	0 - 103	1	6	0.17
Dose Rate	nGy hr^{-1}	2 - 185	16	42	0.38
^{40}K	%	0 - 4.5	0.5	1.1	0.45
^{238}U	ppm	0 - 12	0.7	1.8	0.41
^{232}Th	ppm	0.1 - 41	2.7	6.3	0.43

† CEC is cation-exchange capacity; CCE is calcium carbonate equivalent; Std. Dev. is Standard Deviation; and CV is Coefficient of Variation.

II.2.1.1. Fixed-effect Modeling

The first objective seeks to explain aerial gamma radiometric spatial variability in terms of soil sample information by comparing the mean values of dose rate, ^{40}K, ^{238}eU

and ^{232}eTh with linear fixed-effect or regression models. The methodology draws from the study conducted by Rawlins et al. (2012), but in contrast with their work our focus is to use different fixed-effects or predictors to explain the variation in aerial gamma radiometric data rather than use aerial gamma radiometric data as a fixed effect model itself to explain ground gamma-ray activity. Briefly, a linear fixed-effect model can be defined as:

$$Z = X\tau + \varepsilon, \tag{9}$$

where Z is a matrix of dimensions n x m, where n is the number of observations and m is the number of fixed-effect variables (dose rate, ^{40}K, ^{238}eU and ^{232}eTh); X is a matrix of dimensions n x p, where p is the number of fixed effects or explanatory variables; τ is a vector of coefficients for the fixed, respectively, of dimensions p x 4; ε is a matrix of unexplained residuals of dimensions n x 4 (Rawlins et al., 2012). Individual radioelements were chosen as well as dose rate to address the hypothesis that the individual radioelements will exhibit different characteristics with regard to the individual models.

The following fixed-effects model combinations were used for a given radioelement (dose rate, ^{40}K, ^{238}eU and ^{232}eTh):

1. Mean values of gamma variable p;
2. Mean and clay content;
3. Mean and parent material;
4. Mean and division;
5. Mean and clay content plus parent material;
6. Mean and clay content plus division type;
7. Mean and parent material plus division; and
8. Mean and clay content plus parent material plus division.

For each fixed-effect model, 80 percent of the samples were randomly selected for calibration or training, and the remaining 20 percent were used for a validation, whereby leave-one group-out method was used and repeated 50 times. The goodness-of-fit between the different fixed-effects models was then assessed by calculating and comparing their respective root-mean-squared-errors (RMSE). The aerial gamma radiometric variable that provided a balance in RMSE reduction between the continuous (clay content) and categorical (parent material and physiography) variables was chosen to represent aerial gamma variable for objective 2. For the fixed-effect model using lithology types (model 3), only the eight most common parent materials were used to ensure that their individual parameters could be estimated.

II.2.1.2. National Scale Exploration of Soil Properties and Aerial Gamma Radiometrics

Environmental correlations between a single aerial gamma radiometric variable and soil properties (clay and sand content, CEC, pH and CCE) were first evaluated using simple linear regression models (SLMs) and goodness-of-fit assessed using the adjusted r-squared (R^2) value. Within each soil property, median and the maximum R^2 for a given parent material were calculated and reported within each physiographic division based on results obtained from objective 1 (Figs. 2 and 3). The SLMs were only created for a given parent material if a sufficient sample size criterion was met using the ss.SLR.rho function from powerMediation package in R (DuPont and Plummer, 1998). Soil pH and CCE models, unlike that of texture and CEC, were found to be non-linear and were therefore modeled using generalized linear models under restricted maximum likelihood conditions (Sheather, 2009).

After SLMs were created for all soil properties for all different types of physiography/parent material combinations, suitability maps designating areas of further aerial gamma radiometric exploration for a given soil property were created across the United States based on the R^2 value of a given model. In particular, areas were designated as unsuitable ($R^2 < 0.10$), slightly suitable ($0.10 \leq R^2 < 0.20$), moderately suitable ($0.20 \leq R^2 < 0.30$) or strongly suitable ($R^2 \geq 0.30$), and these criteria were established based on the range in R^2 values across all soil properties.

II.2.1.3. Comparative Analysis of Environmental Covariates to Predict Clay Content

The purpose of creating suitability maps with respect to each soil property is to provide indications of areas where aerial gamma radiometrics can map soils at finer scales. Therefore, we used the clay content suitability map to further explore three different areas classified as 'moderately suitable' or higher were selected in order to assess the performance of aerial dose rate in predicting clay content in comparison with other covariates. These regions indicate different soil forming conditions such as the central High Plains within the state of Texas (Interior Plains physiography), the East Gulf Coastal Plains (Atlantic Plains physiography), and glaciated landscapes located from the northern United States (Interior Plains physiography) (Fig. 2).

The High Plains within Texas are almost entirely dominated by unconsolidated eolian silt and sand sized deposits that were deposited during the Pleistocene epoch (Holliday, 1989). The area has an elevation range between 735 to 1,270 meters above sea level and lies within a semi-arid climate, receiving an annual precipitation between 405 to 560 millimeters. The Coastal Plains within the southeastern United States is characterized by

parent materials such as alluvium and chemical (i.e. limestone) and clastic (sandstone) residuum and marks the old position of the Atlantic Ocean shore during the Mesozoic time period (NRCS, 2006). The Coastal Plains has an elevation range between 30 to 150 meters above sea level, receiving an annual precipitation between 1,345 to 1,550 millimeters. The Glaciated North is characterized by unconsolidated glacial till and glacial rivers attributed to ice sheets that advanced the landscape during the Pleistocene epoch. The Glaciated North has an elevation range between 305 and 625 meters above sea level, receiving an annual precipitation between 405 to 535 millimeters.

Using the environmental covariates described in the previous paragraph, the following models to predict clay content at the soil surface were created under a random 60/40 calibration and validation split, respectively:

1. Gamma radiometric information using regression kriging;
2. Soil sample data only through ordinary kriging;
3. Pre-existing gridded or rasterized soil data from the gSSURGO database;
4. Relief or elevation using regression-kriging;
5. Slope using regression-kriging;
6. Combine all environmental covariates (gSSURGO, relief, elevation, lithology type) under the Cubist model (www.rulequest.com); and
7. Combine all environmental covariates with aerial gamma radiometric data.

Briefly, the Cubist model is a decision-tree model that splits at various nodes and develops leaves of different linear regression models (Wilford et al., 2015). The goodness-of-fit that was used to compare the relative performance of aerial gamma radiometrics against other environmental covariates was RMSE.

II.3. Results and Discussion

Figures 2 and 3 shows that visual correlation exists regionally between aerial gamma radiometric measurements and physiography. For example, high aerial gamma

radiometric (dose rate, ^{40}K, ^{238}eU and ^{232}eTh) estimates occur in the western United States (Rocky Mountains and Intermontane Plateaus), which can contain pyroclastic rhyolitic tuff or ^{40}K-rich acidic rocks ejected from volcanoes between the Miocene and Oligocene time periods (Best et al., 1989). Low amounts of gamma radiation (in particular ^{40}K) occur along the Florida coast (Atlantic Plains) and can be explained by 1) peat deposits, which are known to store high amounts of water, thereby attenuating significant amounts of gamma-rays and 2) parent materials that emit low amounts of gamma radiation such as limestone and sandstone (IAEA, 2003; Beamish, 2015).

II.3.1 Soil Sampling Scheme

The spatial distribution of soil sample locations in the USDA-NRCS database shows clustering or oversampling with respect to division and parent material types (Figs. 2 and 3). This local oversampling is likely a result of participation by the National Cooperative Soil Survey in sampling pedons near Universities and University farms as well as areas of special interest. For example, the University of Illinois (central U.S.) was more involved in collecting and sending their results to the USDA-NRCS (Paul Finnell Sr., personal communication, 2015). Because the sampling is geographically clustered, resulting interpretations of data analysis are skewed or potentially biased towards data-rich areas.

To understand the sampling intensities of the USDA-NRCS database, indices were created to explain the relative proportion of soil samples after stratification into parent materials and physiographic divisions. In order to assess the USDA sampling strategy, proportions of samples were calculated within each parent material and physiography by

dividing the number of samples within a given category by the total number of samples. Additionally, the coefficient of variation (CV) (i.e. standard deviation/mean) within each parent material and physiography type was calculated with respect to dose rate (Kelley, 2007; McKenzie et al., 2008; Beamish, 2014). If the USDA-NRCS sampling strategy is deemed was balanced in terms of areal coverage, the proportion of samples for a given lithology or physiography would be similar to its proportional area across the United States; similarly, the proportion of samples should reflect its CV (i.e. a higher proportion of samples collected from parent materials with a larger CV and vice versa) (Kelley, 2007).

With respect to specific parent materials, soils formed from limestone and dolostone, as well as well as shale have been over-sampled, while sandstone, unconsolidated deposits and basalts have been under-sampled (Table 3). While shales may be one of the most common lithology types across United States, its lower CV suggests that any poor models between aerial gamma radiometrics and soil sample data within clastic parent materials could be explained through an overabundance of shale soils. With respect to physiography, the Interior Highlands, Pacific Mountains and the Interior Plains are well sampled; in contrast, soils from the Intermontane Plateaus, Atlantic Plains, and Appalachian Highlands are sparsely sampled (Table 3).

The implication from the NCSS-SCD unbalanced sampling scheme is that any statistical model that uses aerial gamma radiometric data and the NCSS-SCD across the conterminous U.S. will tend to reflect aerial gamma radiometrics and soil relationships found within the most highly sampled areas. The sampling design is also limited in

utility because the disproportionate amount of samples with respect to parent material type makes any trends between soil properties and aerial gamma radiometric trends difficult, as models from higher amounts of samples are based on more information (i.e. higher degrees of freedom), and vice-versa.

Table 3. Sampling statistics in terms of areal proportion across the United States and coefficient of variation (CV), expressed in terms of soil parent material.

Category	**Proportion of soil samples**	**Areal Proportion of U.S.**	**CV (Dose Rate)**
		Parent Material	
Residuum, Clastic Sedimentary	7	22	0.39
Alluvium	25	16	0.41
Glacial Till	20	14	0.25
Residuum, Igneous/Metamorphic Undifferentiated	19	11	0.58
Eolian	3	7	0.30
Colluvium	11	6	0.24
Glaciofluvial	4	5	0.34
Resdiuum, Chemical Sedimentary	8	4	0.32
		Physiography	
Laurentian Upland	2	1	0.32
Atlantic Plain	8	15	0.38
Appalachian Highlands	9	11	0.30
Interior Plains	48	37	0.27
Interior Highlands	7	2	0.28
Rocky Mountain Systems	5	8	0.32
Intermontane Plateaus	11	20	0.44
Pacific Mountain Systems	8	6	0.55

II.3.2. Fixed Effect Model Results

The fixed-effect models were used to identify what source information the aerial gamma radiometric data might be most useful in mapping soils across the U.S. and to

identify which spatial delineation, parent material or physiographic division, is more useful in classifying regions where aerial gamma radiometrics works best. In general, the RMSE between predicted and measured values of both ^{40}K and dose rate were most reduced by the addition of the fixed effects, while ^{238}U was least affected by the addition of fixed-effects (Table 4). Table 4 indicated that much of the ^{40}K variability could be explained in terms of physiography, and were subsequently compared with that of parent materials (Fig. 4). ^{40}K concentrations in particular were more highly variable within physiographic divisions than parent materials because the former are characterized by parent materials with more highly contrasting aerial gamma radiometric signatures, while the latter exhibits less separation in ^{40}K concentrations perhaps due to similar mineralogy types (Fig. 4).

Adding clay content as a fixed-effect reduced the RMSE values of dose rate and ^{232}Th relative to the initial model by 2.9 and 3.7%, respectively, and although its reduction was less than that of physiography, it was an improvement over the addition of parent material (Table 5). ^{232}Th in contrast with dose rate, ^{40}K, and ^{238}U produced the relatively highest reduction in RMSE when clay content alone was added because ^{232}Th is readily adsorbed onto clay minerals (Wilford, 2012).

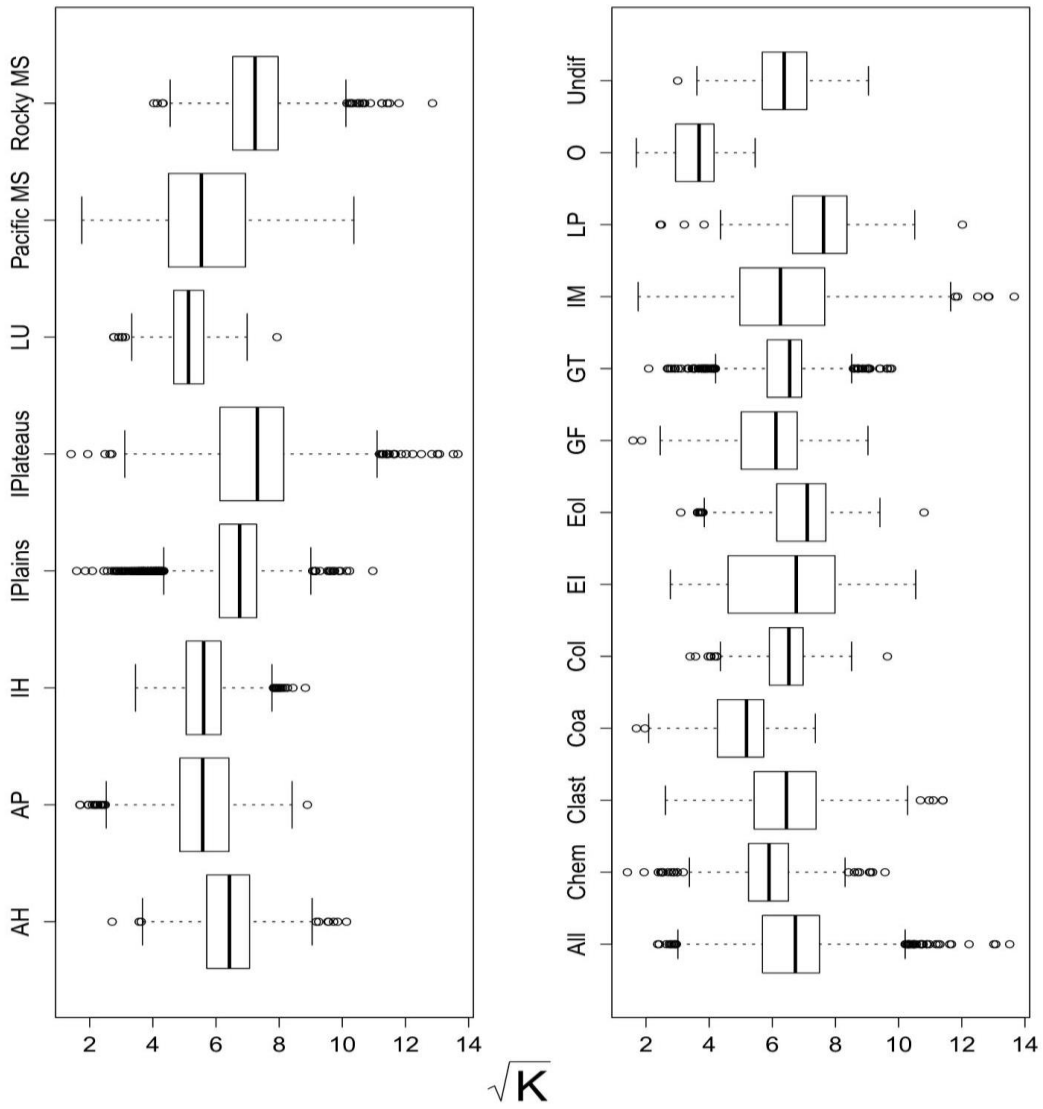

Figure 4. Box and whisker plots comparing ^{40}K soil sample variability based on physiographic division (left, ref. Fig. 2) and parent material (right) groupings. The abbreviated physiographic division codes used here represent the regions shown in Figure 2: AH = Appalachian Highlands, AP= Atlantic Plains, IH = Interior Highlands, IPlains = Interior Plains, IPlateaus = Intermontane Plateaus, LU = Laurentian Uplands, Pacific MS = Pacific Mountain Systems, Rocky MS = Rocky Mountain Systems. The abbreviated parent material codes used here represent the following parent materials from Figure 3: All = Alluvium, Chem = Residuum, Chemical Sedimentary, Clast = Residuum, Clastic Sedimentary, Coa = Coastal, Col = Colluvium, EI = Residuum, Extrusive Igneous, Eol = Eolian, GF = Glaciolfluvial, GT = Glacial Till, IM = Residuum, Igneous/Metamorphic Undifferentiated, LP = Lacustrine/Playa, O = Organic, Undif = Undifferentiated Residuum/Alluvium/Colluvium.

Table 4. Results for fixed effect models expressed as the root-mean-squared error for each aerial gamma radiometric variable across the United States.

Fixed Effect Model[†]	Dose Rate		^{40}K		^{238}U		^{232}Th	
	RMSE	% Diff.	RMSE	% Diff.	RMSE	% Diff.	RMSE	% Diff.
	nGy hr^{-1}				ppm		ppm	
1. Mean value	17.6	-	0.57	-	0.77	-	2.41	-
2. Mean + Clay	17.4	0.9	0.57	0.0	0.77	0.0	2.32	1.4
3. Mean + PM	17.2	2.1	0.55	3.5	0.76	1.3	2.36	1.7
4. Mean + Division	17.0	3.0	0.54	5.3	0.75	2.6	2.27	3.1
5. Mean + Clay + PM	15.7	10.8	0.47	17.5	0.73	5.2	2.28	6.5
6. Mean + Clay + Division	15.6	11.4	0.47	17.5	0.72	6.5	2.20	7.5
7. Mean + PM + Division	15.4	12.5	0.46	19.3	0.72	6.5	2.22	8.2
8. Mean + Clay + PM + Division	15.3	13.0	0.46	19.3	0.71	7.8	2.14	9.2

[†] PM is Parent Material or generalized lithology from Fig. 2; Division is the physiographic division name from Fig. 3; and % Diff. is percent difference between the RMSE of a given fixed-effect model and the initial mean RMSE.

The fixed effects with the most influence in estimating means based on the highest percent reduction in RMSEs were (in order): physiographic division, parent material and clay content, although higher percent differences in aerial gamma radiometric RMSE occurred when multiple fixed effects were included in the model (Table 4). Physiography was effective in explaining variations in ^{40}K not only in terms of parent materials, but because physiography accounts for climatic spatial variability as well. Weathering mechanisms such as hydrolysis can aid in the mobility of ^{40}K within a landscape and can thus be used to additionally explain aerial gamma radiometric patterns (Bierwirth, 1996). Therefore, these results suggest that relationships between aerial

gamma radiometrics and soil properties can be improved after considering soils and their parent material types located or nested within a given physiographic division.

II.3.3. National and Regional Scale Exploration

Results from the fixed-effects models suggest that dose rate and ^{232}Th are good choices for mapping soil properties because, once physiographic division was included as a fixed effect, adding clay content further reduced the RMSE of dose rate and ^{232}Th (Table 4). Although ^{232}Th provided a higher reduction in RMSE with the addition of clay content, dose rate was chosen to represent aerial gamma radiometrics in creating the soil property suitability maps because it contains information on physiography (^{40}K) as well as clay content (^{232}Th) (Wilford et al., 1997).

Figures 6a-6e show suitability maps based on R^2 values for soil properties (i.e. clay and sand contents, CEC, CCE, pH) and aerial dose rate within different physiography and parent material combinations. In terms of spatial coverage, soil texture along with CEC show the highest amount of areas suggesting further aerial gamma radiometric exploration because these properties are most closely associated with original parent material mineralogy signatures. Furthermore, these properties are typically static in nature, meaning that their variability is more associated with natural soil forming conditions in contrast with CCE and pH which show the lowest amount of areas suggesting possible influence in terms of soil management such as the addition of fertilizers and/or lime, which can affect not only the variability of pH and CCE but radioactivity as well (Bouma and Finke, 1993; Boukhenfouf, 2011).

Regardless of soil property, there are a low amount of areas classified as strongly suitable for further exploration and as such requires further discussion. As Ryan et al. (2000) explains, a low Adj. R^2 using environmental correlation modeling can be a result of three causes: (1) a natural poor relation; (2) the data feature space is very small compared to its possible predicted values; and (3) the presence of extreme local soil variation. With respect to the first cause, legacy aerial gamma radiometrics suffers from a poor resolution because of survey conditions such as relatively high altitude sensors (120 meters) and a large distance between flight lines (i.e. 2, 5 and 10 kilometers according to Duval et al. (2005)). The NCSS-SCD spatial distribution contributes to this issue because most soil samples were collected outside of the footprint represented by the aerial gamma detector or lie between adjacent survey transect lines, suggesting additional uncertainty in soil aerial gamma radiometric abundances (Beamish, 2014). The second cause is usually not problematic, as there are a high number of samples within each division, although some areas are more variable than others (Fig. 4). The third cause cannot be answered from the methodology employed here, as a spatial average of soil samples would be required. Therefore, we conclude that the first cause is the most likely explanation for the moderate-weak relationships shown from the suitability maps of Figure 6, although such correlations are expected to improve at larger spatial scales.

II.3.3.1. Texture (Clay and Sand Content)

A suitability map for clay content (Figure 5) indicates that aerial gamma radiometrics can potentially map clay content within unconsolidated parent materials

such as eolian, alluvial, coastal and glacial sediments, as well as chemical and clastic sedimentary residuum located within the Interior Plains (IV) and Atlantic Plains (II) (Figs. 3 and 5). Within these two physiographic divisions, aerial gamma radiometrics can map clay content because these parent materials give different signals depending based on mineralogy. For example, soils low in clay content for glaciofluvial deposits within the Interior Plains were classified as siliceous or poor in radioelemental abundance, whereas high clay soils were classified as illitic or high radioelemental content (Wilford et al., 1997). Therefore, moderate or strong suitability classifications with respect to clay content are dependent on the range of mineralogy types that occur within a given parent material.

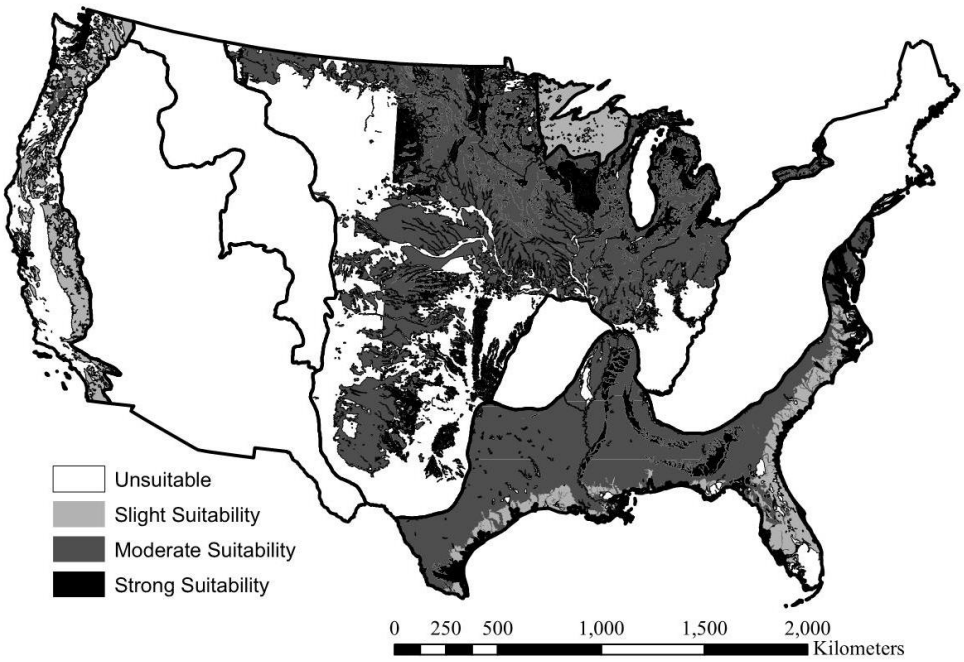

Figure 5: Suitability maps for further aerial gamma radiometric exploration for clay content models under different physiography/parent material combinations.

Significant relationships between dose rate and clay were relatively high within the Atlantic Plains and the Interior Plains because these areas are characterized by relatively flat topography, where changes in dose rate are typically associated with changes in clay or soil formation. In contrast, areas associated with higher variability in topography such as the Appalachian Highlands, Interior Highlands, Rocky Mountain Systems and Intermontane Plateaus do not contain any parent materials classified as suitable for further exploration due to soil processes such as erosion which can transport ^{40}K, ^{238}U and ^{232}Th downslope and thus modify the original gamma signal.

Although aerial gamma radiometrics was a poor predictor of clay content in areas with more variable topography, it could map clay content within the Pacific Mountain Systems due to the presence of organic carbon. Rawlins et al. (2009) explained that soil organic carbon can cause a decrease in dose rate emissions because organic materials can accumulate water (and thus attenuate gamma-rays) and/or simply reduce the amount of mineral content available. A majority of the soils forming from igneous parent materials in the area (i.e. classified as 'slightly suitable') were classified as andisols according to USDA Taxonomy, and such soils can accumulate high amounts of soil organic carbon (Nanzyo, 2002).

A suitability map for sand content is shown in Figure 6 and generally overlaps with clay content suitable areas such as the Atlantic and Interior Plains (Fig. 5) because within these landscapes sand sized particles are either characterized by low gamma abundant minerals such as quartz or high gamma abundant minerals within the clay

and/or silt sized fractions (Mahmood et al., 2013). For example, the r-squared value between sand content and dose rate for eolian deposits within the Atlantic Plains was very high ($R^2 = 0.74$) because of sharply contrasting sand and dose rates located within the southern Texas sand sheet (high sand, low gamma abundance) and loess deposits adjacent to the Mississippi River (lower in sand, higher in silts) which have a relatively higher abundance in dose rate due to the presence of potassium feldspars and/or trace minerals rich in ^{238}U and ^{232}Th such as zircon (Heinrich, 2008).

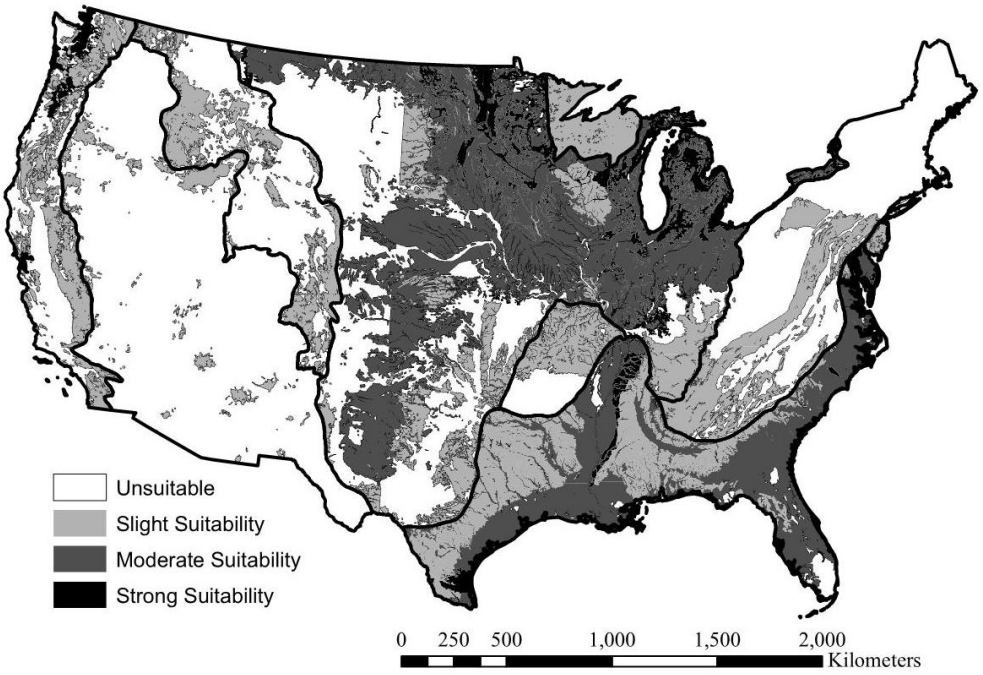

Figure 6: Suitability maps for further aerial gamma radiometric exploration for sand content models under different physiography/parent material combinations.

Although overlapping of suitability occurred between sand and clay content maps, there were several areas where sand content suitability diverged from clay content such as the Appalachian and Interior Highlands, as well as the Rocky Mountain systems. Within the Appalachian and Interior Highlands, sands were classified as 'slightly suitable' and clays unsuitable for further aerial exploration because the source of radiometric content lies within both the clay- and silt-sized fractions, while the Rocky Mountains predominantly the silt-sized fraction ($R^2 = 0.25$ for silt and dose rate within igneous and metamorphic residuum, Figure 3). Therefore, relationships between sand content and aerial dose rate can be established if the gamma radiometric source is located either within the clay- or silt-sized fractions, further suggesting that relationships between clay content and dose rate are more restrictive in nature.

II.3.3.2. Cation Exchange Capacity

The cation-exchange capacity (CEC) suitability map United States indicates that relationships with aerial dose rate in general are poorer compared with that of clay and sand contents (Figure 7). Relatively lower R^2 values for CEC and dose rate were found due to differences in the source of CEC. For example, in areas where clay content defines CEC (i.e. Atlantic Plains), a strong suitability classification was given whereas areas where clay and organic material content both contribute to CEC (i.e. organic rich soils within the Interior Plains and Pacific Mountain Systems) were predominantly classified as slightly suitable. As previously discussed, soils rich in organic material can hold large amounts of water which can attenuate emitted gamma-rays from the soil. Additionally, when clay minerals and associated ^{40}K begin to weather and eluviate from

the soil, ^{232}Th and ^{238}U can be retained by soils rich in organic matter, leading to a poorer relationship between the two variables (Wilford, 2012).

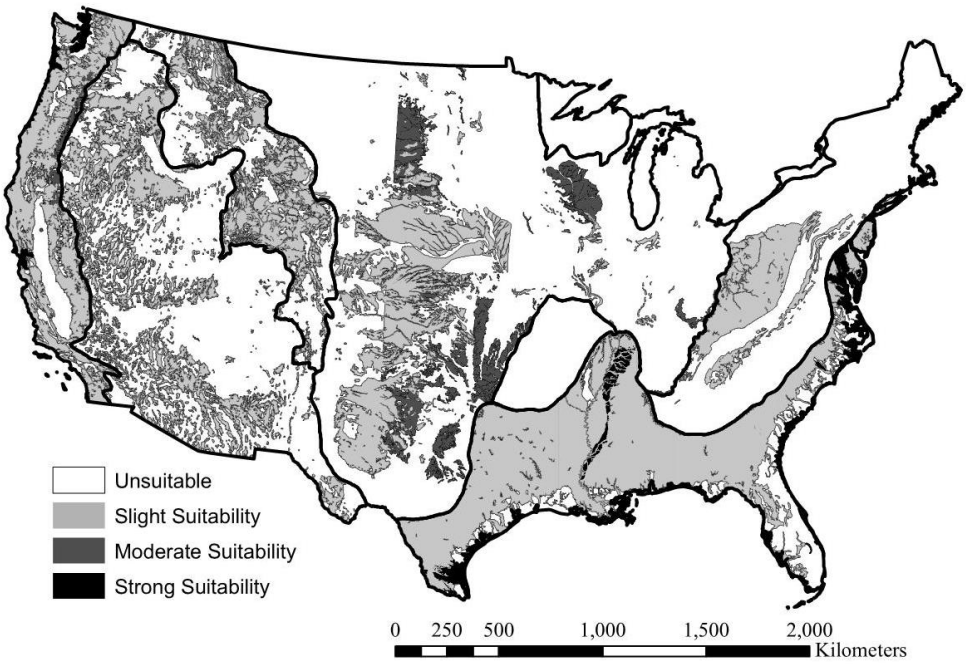

Figure 7: Suitability maps for further aerial gamma radiometric exploration for CEC models under different physiography/parent material combinations.

II.3.3.3. Calcium Carbonate Equivalent

Calcium carbonate equivalent (CCE) suitability coverage differed from that of texture and CEC in terms of total coverage as well as locations of suitable areas (i.e. Intermontane Plateaus and Pacific Mountain Systems) (Fig. 8). The areas classified as 'strongly suitable' are characterized by desert environments (such as the Grand Canyon) with low water contents and therefore low leaching potential. A limited leaching

environment allows for the presence of to accumulate calcium carbonates on the soil surface which can dilute the overall aerial gamma radiometric signal and therefore allowing for mapping of CCE, assuming aerial gamma radiometrics and texture correlations are low (Stahr et al., 2013). For example, a significant relationship between CCE and dose rate occurred for soils forming from chemical sedimentary residuum found within arid environments (VII) correlations and aerial gamma radiometric correlations with clay content were low ($\rho = 0.00$). The soils within this area with relatively abundant carbonates were classified as carbonatic mineralogy according to and were heavily depleted in ^{40}K, ^{238}U and ^{232}Th, while the soils lower in carbonates were characterized as smectitic (or gamma-rich) mineralogy.

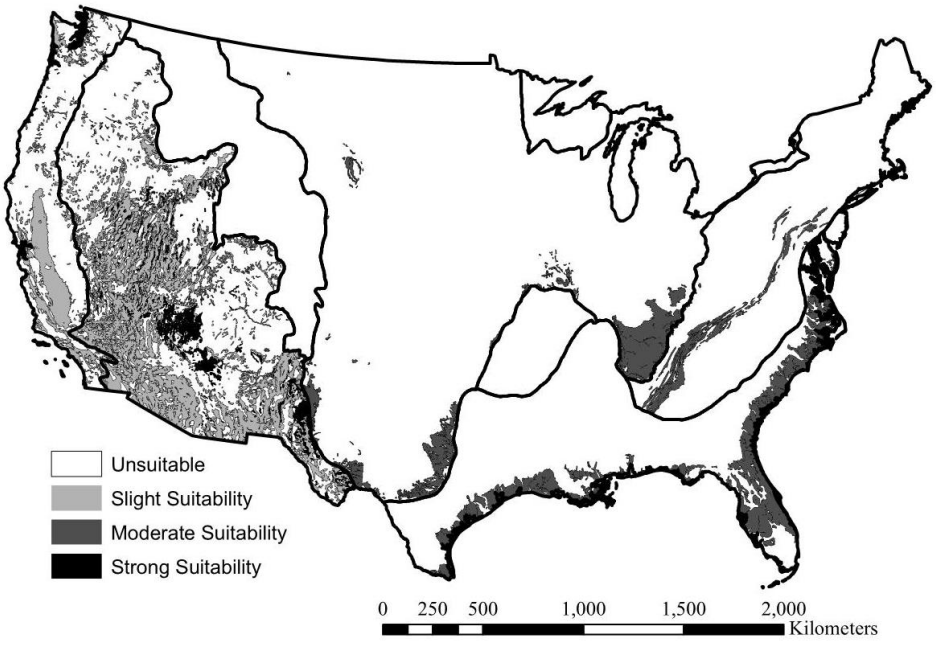

Figure 8: Suitability maps for further aerial gamma radiometric exploration for calcium carbonate equivalent (CCE).

II.3.3.4. pH

The most strongly suitable regions according to pH and dose relationships exhibited positive trends and were located within Pacific Mountain System alluvial sediments because of the acidic conditions due to high rainfall conditions and conifers located in the most northwestern states (i.e. Washington state) (Fig. 9). Relationships between pH and dose rate were generally positive because ^{238}U and ^{232}Th become soluble under acidic conditions and are adsorbed to clay surfaces (Petersen et al., 2012). Within Pacific Mountain System alluvial sediments, pH appears to respond to changes in carbonates (Fig. 8), although pH variability (and therefore suitability) can be affected by sources other than CCE. For example, alluvial sediments within the Atlantic Plains unlike that of CCE were classified as 'moderately suitable' for further exploration because this area is more associated with the suitability maps for clay and sand content than CCE. However, other areas such as the Interior Plains that responded to changes in texture (Figs. 5-6) were classified as unsuitable with respect to pH possibly due to the influence of land management practices.

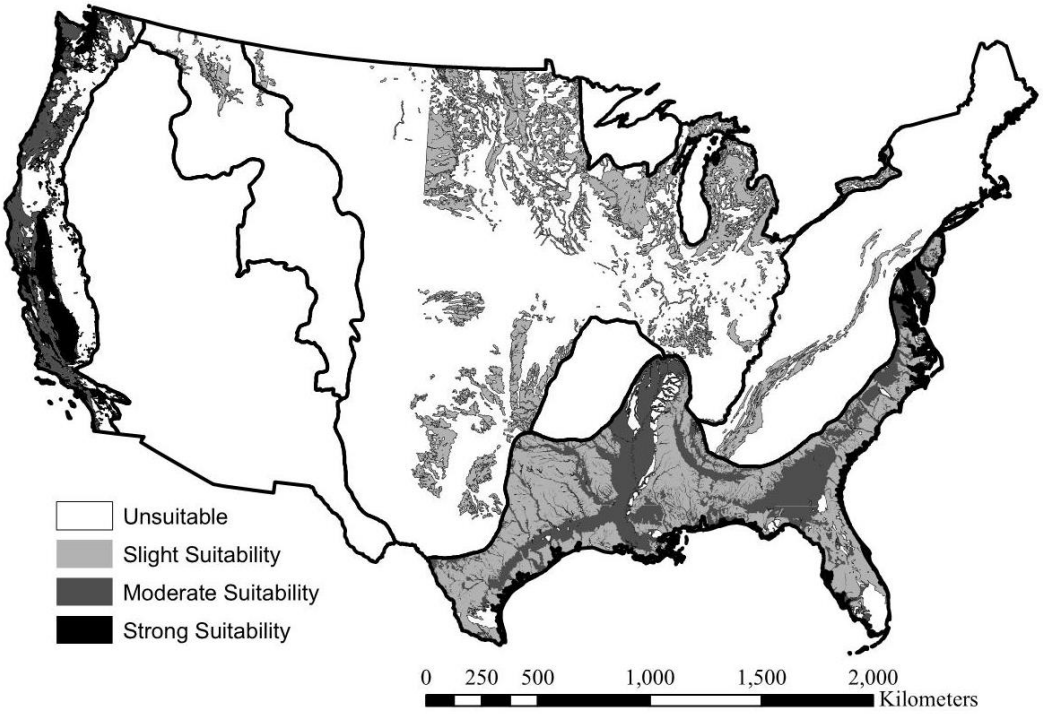

Figure 9: Suitability maps for further aerial gamma radiometric exploration for pH.

II.3.4. Comparative Analysis of Digital Environmental Covariates

The purpose for exploring relationships between soil properties and aerial gamma radiometrics is, in part, to assess its suitability as a covariate to interpolate soil properties across the United States. The previous analysis suggested that such assessments are ideal only when considering region-specific areas as well as the parent materials within each region. Previous analysis of comparing dose rate with soil samples and their properties (such as clay content) indicated that areas located within flat topographies, while those from more variable topography were less correlated, regardless of parent material type. These flat landscapes were generally classified as ‘moderately suitable’ or ‘strongly suitable’ and three areas were therefore selected as characterized in the methodology for

further aerial gamma radiometric exploration, particularly in predicting clay content compared with other SCORPAN covariates such as elevation, slope and gSSURGO.

Validation results after applying the different predictive models are shown in Table 5. Within the High Plains, the performance of aerial dose rate in predicting clay content using regression-kriging (RK) surpassed that of ordinary kriging (OK) or from other environmental covariate regression-kriging models, despite the relatively coarse line-spacing distances set in the original survey (i.e. 5 km). In addition to higher accuracy, the incorporation of dose rate reduced the bias under the Cubist model (-3.6 to -2.4%, respectively, Table 5). Dose rate was also more accurate in predicting clay content in the High Plains because the area is primary characterized by unconsolidated eolian deposits that provide different gamma radiometric signatures in terms of mineralogy such as K-feldspar (gamma-rich) and quartz (gamma-poor) (Muhs and Holliday, 2001).

In contrast with the High Plains, dose rate models within the Glaciated North and the Coastal Plains were less accurate than OK and/or non-gamma radiometric RK models (Table 5). The mixed results of the gamma radiometric RK models compared with OK or non-gamma radiometric models can be explained through several sources. First, the gamma radiometric data in these two areas were collected at coarse line-spacing distances (10 km) and therefore contain a lower signal to noise ratio compared with surveys from the High Plains (5 km). Second, the two areas did not consist of a uniform parent material as in the High Plains, and it is therefore possible that unsuitable parent materials according to figure 6a could degrade the dose rate RK models, especially if these ‘unsuitable’ parent materials were preferentially sampled.

Table 5. Validation results from spatial prediction models of surface soil clay content for the High Plains in Texas, Coastal Plains and Glaciated North using environmental covariates. Goodness-of-fit statistics are expressed in terms of adjusted R^2 (R^2), Root Mean Squared Error (RMSE), and bias.

Model†	High Plains (n = 64)			East Gulf Coastal Plains (n = 158)			Glacial North (n = 125)		
	R^2	RMSE	Bias	R^2	RMSE	Bias	R^2	RMSE	Bias
DR	0.33	11.7	-2.0	0.28	13.9	-4.0	0.32	9.1	-0.3
Clay content	0.27	12.3	-2.8	0.23	15.7	-5.8	0.38	8.8	-0.4
gSSURGO	0.20	12.9	-4.2	0.44	12.0	-1.5	0.48	8.0	-0.6
Elevation	0.26	12.5	-2.5	0.25	14.3	-2.7	0.38	8.9	-0.4
Slope	0.27	12.4	-2.3	0.22	15.8	-5.8	0.39	9.0	-0.4
All Covar.-no DR	0.49	10.3	-3.6	0.44	12.0	-1.5	0.48	8.0	-0.6
All Covar.-w. DR	0.47	10.2	-2.4	0.48	11.5	-1.9	0.45	8.2	-0.6

† DR = dose rate; All Covar. = All covariates. All models except clay content (ordinary kriging) were conducted using regression-kriging.

II.4. Conclusions

The purpose of this study was to analyze relationships between legacy aerial gamma radiometrics and soil datasets across large spatial scales. Under the hypothesis that the spatial distribution of aerial gamma radiometric patterns are affected by parent-material and physiography types, a legacy soil database was selected and spatially joined with a physiography and reclassified lithology maps in an attempt to link soil property with aerial gamma radiometric data across the United States.

Initial investigations towards the spatial distribution of the legacy soil samples indicated an unbalanced sampling scheme, and samples were biased towards soils

forming from clastic sedimentary rock, especially within the central-northern United States, based on relative areal proportions and coefficient of variation calculations. The locations of the samples proved to be problematic in terms of the gamma radiometric response, as most samples were not collected based on initial surveys.

To link aerial gamma radiometrics with soil properties, a fixed-effect model analysis was conducted to identify all sources of gamma (dose rate, ^{40}K, ^{238}U, ^{232}Th) variation. The addition of clay content as a fixed effect term lowered the RMSE in the estimation of these aerial gamma radiometric variables up to 1 %, and up to 4 and 19 % when incorporated with lithology and physiographic groups respectively, suggesting that aerial gamma radiometrics are best explained in terms of physiographic and parent material units as well as clay content across the United States.

Aerial gamma radiometric data, in particular dose rate, was found to be related to with soil properties such as texture (clay and sand contents), cation-exchange capacity, and in certain regions calcium carbonate. Clay content in general provided the strongest linear relationships with aerial gamma radiometrics regardless of parent material, while sand content exhibited similar but opposite trends, although trends for both variables were dictated by soil composition (i.e. organic carbon, clay mineralogy) and regions of similar geomorphic landscapes. Linear models for Cation-exchange capacity relationships were similar but generally weaker than that of clay content due to areas where organic material contributes to CEC such as within the northwestern United States. Relationships between calcium carbonate were weak except within arid landscapes in the western United States. The generalized landscapes in which aerial

gamma radiometrics was most strongly related with soil properties were found for soils locate over flat terrains with parent materials that provided contrasting gamma-ray responses.

Comparative analysis between aerial gamma radiometrics and digital environmental SCORPAN covariates (i.e. slope, lithology, gSSURGO clay estimates) in predicting clay content through regression- and ordinary-kriging modeling indicated that gamma data was a useful tool that can be implemented over flat terrain soils, but results were mixed when compared with digital covariates.

Further investigations are needed towards verifying the data quality of the aerial gamma radiometric maps provided by United States Geological Survey (USGS) and one such approach could begin with the initial surveys. For example, transect lines conducted at various line-spacing distances (2, 5 and 10 km) across the United States are currently available alongside the gridded data and could be validated by conducting surveys where the gamma-ray sensor is located much closer to the ground. The success of these different survey methods, however, is only useful to the extent that ground surveys are mapping soil properties, and we have shown here that such relationships can be strong, especially within a given set of physiography and parent material types.

CHAPTER III

UNDERSTANDING AERIAL GAMMA RADIOMETRICS THROUGH PROXIMAL SURVEYS

III.1. Introduction

Reliable and accurate soil information is needed for assessing soil capability not only at the m-scale but across regions at the 1,000 to 10,000 km scale. For example, initiatives such as the GlobalSoilMap.net project are working to map five soil properties (clay, sand, bulk density, pH, carbon) at a 1-arc second scale (Arrouays et al., 2014), and land surface and hydrology modeling projects are running at finer and finer resolutions because of accessibility of computing power (Wood et al., 2011; Cheney et al., 2015). Aerial gamma-ray radiometrics have been proposed to accomplish such a task because it indicates spatial variations in soil minerals as well as changes in weathering intensity due to differences in landscape position (Wilford, 2012; Beamish, 2013; Arrouays et al., 2014; Stockmann et al., 2015). In aerial gamma radiometrics, a sensor is placed at large altitudes (120 m) and detects gamma radiation passively emitted by unstable radioelements within the soil due to radioactive decay and include elements such as potassium (^{40}K, 1.46 MeV), uranium (^{238}U, 1.76 MeV) and thorium (^{232}Th, 2.62 MeV) (Minty, 1997b). Collectively, these three naturally occurring radioactive materials have successfully been used to differentiate soil types and associated attributes such as texture and calcium carbonate over regional areas (Bierwirth, 1996; Beamish, 2015; Wilford et al., 2015). However, these studies have been confined to aerial gamma radiometrics

collected in Australia and the United Kingdom, and there is currently a lack of understanding between pre-existing aerial gamma radiometrics and soil properties across the conterminous United States (Minty, 2009; Stockmann et al., 2015).

Initial assessment and validation of legacy gridded data available in the U.S. provided by the United States Geological Survey (USGS) (Chapter II) indicated weak relationships with geo-referenced lab characterized soil properties of clay, CEC, sand, and inorganic carbon, even after stratification into physiography and subsequent parent materials across the U.S. The relationships between aerial gamma radiometrics and soil data were thought to be poorly distinguished partly because of the unbalanced sampling design, naturally associated with such a legacy database. Within a given physiography or parent material, the spatial distribution of soil samples in the National Characterization Soil Survey-Soil Characterization Database (NCSS-SCD) were not ideal for querying the extremes of the aerial gamma radiometric response. In other words, the soil samples were not stratified by aerial gamma radiometric response and can be quite clustered within different physiography and parent material types.

One of the assumptions made within Chapter II that was critical in analyzing relationships between aerial gamma radiometric soil properties was that aerial gamma radiometric data are representative of emissions located on the ground, at the location the pedon was sampled. This assumption, however, is weak because of the gridded aerial gamma radiometric maps for the US are inherently low in spatial resolution due to coarse line-spacing distances (5 and 10 km in the US compared with 0.4 km in Australia) and high altitudes (120 m in the U.S. compared with 80 km in Australia). A

high altitude sensor results in a large footprint or field-of-view (an ellipse of dimensions 265 x 378 m), and a relatively large FOV implies that soil heterogeneities become spatially averaged due to differences in support volume with regard to single soil samples (pedons) and aerial gamma radiometrics. Therefore, there is a need to test the quality of this aerial gamma radiometric data in the United States as well as understand how useful aerial gamma radiometrics can be to soil mapping. The relevance of validating the USGS aerial gamma radiometrics database lies within recent digital soil mapping efforts which have used a rasterized aerial gamma radiometric dataset as a soil environmental covariate for digital soil class and property predictions (Odgers et al., 2015; Cheney et al., 2015).

In an ideal experiment, gamma measurements provided by an aerial gamma spectrometer would be validated by collecting a statistically representative amount of soil samples within the footprint of an aerial gamma radiometric sensor (Cardarelli II et al., 2011). As well, the methodology should include a design that stratifies the sampling with respect to aerial gamma radiometric response (Minasny and McBratney, 2006; Cardarelli II et al., 2011). An alternative data collection method that can be used to ground-truth and understand aerial gamma-ray data could be to conduct a vehicle-traversed, on-ground or proximal gamma radiometric survey. A proximal gamma radiometric survey can be used to collect a high resolution gamma radiometric pattern that can be used for soil sampling and averaging up to the aerial footprint. As well, the support volumes of a single soil sample and proximal gamma radiometric data are more similar. Vehicle-traversed systems are not entirely without limitation, however, for they

are limited in spatial scope and are inhibited by obstacles such as fences and property boundaries (Stockmann et al., 2015).

Initial analysis of ground-truthing aerial gamma radiometrics with proximal data within literature suggests that comparisons between aerial gamma radiometrics and proximal gamma radiometrics are most successful when the aerial gamma radiometric data is variable in itself. For example, Kock and Samuelsson (2011) compared aerial gamma radiometric point measures collected by the Geological Survey of Sweden with backpack or foot-traversed proximal gamma radiometric measurements (i.e. ^{40}K, ^{238}U and ^{232}Th) from three different landscapes in southern Sweden, and in their results they found that ^{238}U and ^{232}Th measurements were most successful (R^2 of 0.82 and 0.79, respectively) when at least one site within each radioelement exhibited large amounts of variability. Therefore, comparisons of aerial and proximal gamma radiometrics should be most successful either within one parent material undergoing differential weathering conditions or between parent materials providing contrasting radiometric signatures.

While proximal and aerial gamma radiometric comparisons will provide an indication of aerial gamma radiometric agreeability between the two survey methods, their comparisons are only meaningful from a soil science context if proximal gamma radiometric data are mapping spatially variable soil properties, and recent literature has indicated such relationships can be established. For example, Priori et al. (2014) correlated the ^{40}K, ^{238}U and ^{232}Th energy windows with soil texture across three parent materials in Italy (i.e. flysch, sandstones and marine alluvial deposits). Additionally, Viscarra-Rossel et al. (2007) mapped clay content, nutrients (K, Fe), pH, and salinity in

two different soil settings (i.e. residual and alluvial parent materials) in Australia using hyperspectral GR. Various adjusted R^2 values were reported, with silt content, fine sand, K and Fe concentrations lowest in adjusted R^2. These investigations demonstrate the site-specific nature of gamma radiometrics regardless of selected soil properties, as well as the best representation (i.e. individual or combined energy windows) of gamma radiometrics in predicting soil properties within various parent materials, but such applications to our knowledge are non-existent for soil landscapes within the U.S.

The overall goal of this investigation is to improve our understanding of aerial gamma radiometrics collected over different parent materials within the United States. To achieve this goal, proximal gamma radiometric surveys and soil samples were collected over three parent materials and co-located with aerial gamma radiometric transect lines. We hypothesize that aerial gamma radiometric responses are more strongly related to soil properties than can be shown using legacy soil survey databases and that the relationship (i.e. strength and type) between aerial gamma radiometrics and soil properties varies with parent material.

To test our hypotheses, two specific objectives are addressed. First, assess the strength of relationships between laboratory derived soil properties and proximal gamma-ray spectral data on a field-scale using Pearson correlation coefficients and multiple linear regression modelling; and second to compare the spatial patterns between proximal and aerial gamma-ray spectrometer data (e.g. dose rate, ^{40}K, ^{238}U and ^{232}Th) through scatter plots and analysis of covariance.

III.2. Materials and Methods

III.2.1. Site Descriptions

Four sites in three different locations were chosen for proximal gamma radiometric surveys within the state of Texas (Fig. 10). The site selection criteria included accessing different parent materials and capturing variability in the raw aerial gamma radiometric point data in Central Texas. These sites represent several parent materials located within the region, including alluvium (young and old) as well as residuum (shale, sandstone and marl). Because of the far distance between aerial gamma radiometric survey transects, only one transect line was chosen and analyzed at each parent material site.

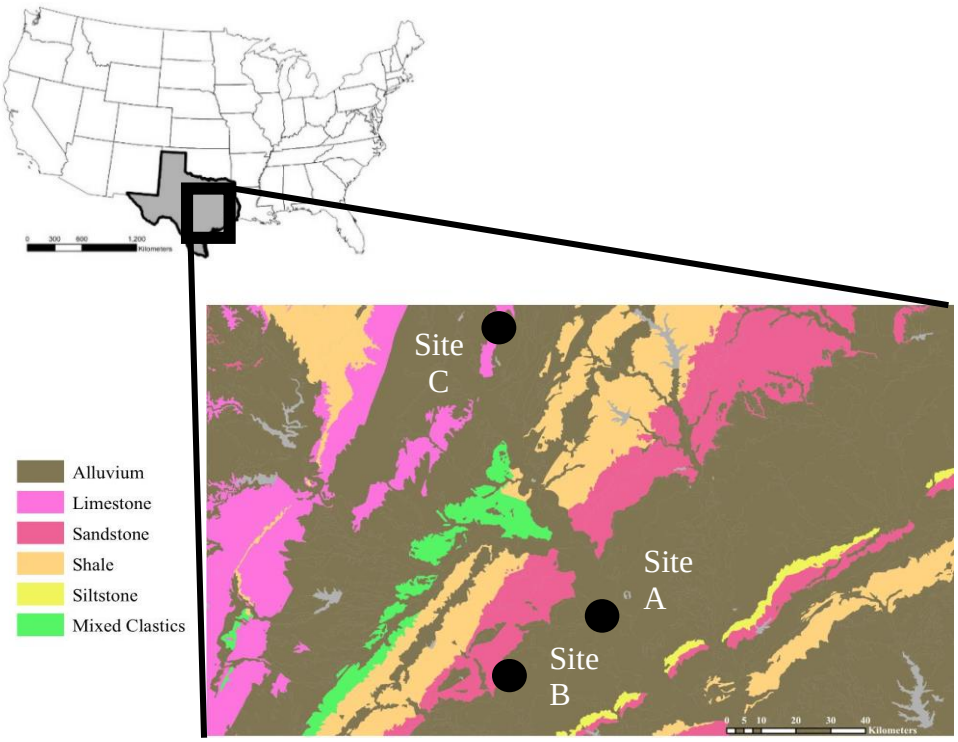

Figure 10. Geographical locations of the three proximal gamma radiometric surveys described within the text.

Site A includes approximately 895 ha (30°39'59.07"N, -96°32'44.92"W) nearby the Brazos River and contains soils deposited onto a nearly-level floodplain within the last 2000 years (Waters and Nordt, 1995; Chervenka, 2002). The original source of these sediments are found within the Blackwater Draw Formation within the southern High Plains and contain mixed mineralogy (Holliday, 1989). Surface soil textures are mapped as clay, silty clay loam, and silt loam according to the USDA Soil Survey (Soil Survey Staff, 2014a; Fig. 11a). The soil classifications are Very-fine, mixed, active, thermic Chromic Hapluderts, Fine, fine-silty mixed, superactive, thermic Udifluventic Haplusteps, Coarse-silty, Coarse-Loamy, mixed, superactive, calcareous, thermic Udic Ustifluvents. The primary land use for soils in Site A is irrigated and dryland cropping of corn and cotton with conventional tillage. The average annual precipitation is 99 centimeters.

Site B is approximately 156 ha (30°29'7"N -96°50'59"W) and contains soils formed on uplands over discrete and interbedded shale and sandstone residuum (Jurena, 2005; Fig. 11b). These bedrock types were initially deposited in shallow marine environments around the Eocene geologic time period, between 50 and 36 million years ago when an ancient sea transgressed the Texas land mass (Jurena, 2005). The soil surface textures mapped are loam, loamy fine sand, fine sandy loam, fine sand, sandy clay loam, and clay (Soil Survey Staff, 1999). The soil classifications are Fine, Fine-loamy, loamy, siliceous, smecitic, mixed, active, semi-active thermic Arenic, Grossarenic, Ultic, Udertic, Psammentic Paleustalfs; Fine, smectitic, thermic Udertic Argiustolls; and Fine,

smectitic, mixed, thermic Udic Haplusterts. The Alfisols at this site form from parent materials rich in glauconite, an iron potassium phyllosilicate indicative of shallow-marine environments (Triplehorn, 1965; Jurena, 2005). The primary land use is pastureland, and the average annual precipitation is 97 centimeters.

Site C consists of two regions, termed C1 and C2 and are located under the same aerial transect line (Figs. 11c and 11d). Site C1 is approximately 184 ha (31°27'36"N - 96°52'50"W) and contains soils formed on uplands consisting of marl (or carbonate-rich shale) residuum; while site C2 contains both upland marl and old alluvium or terrace landforms from the Brazos River. The primary soil surface textures in C1 are clay and silty clay; while at site C2, the surface textures are clay, silty clay loam, silty clay and clay loam. Soils at classifications at C1 are classified as Fine, smectitic, thermic Udic Haplusterts and Fine-silty, carbonatic, thermic Udortherntic Haplustolls; at C2, classifications additionally include Fine, smectitic, thermic Oxyaquic, Udertic Vertic Haplustalfs. The land-use for both sites C1 and C2 is corn, and the annual precipitation in the area is 85 centimeters (Soil Survey Staff, 1999; Miller and Greenwade, 2001).

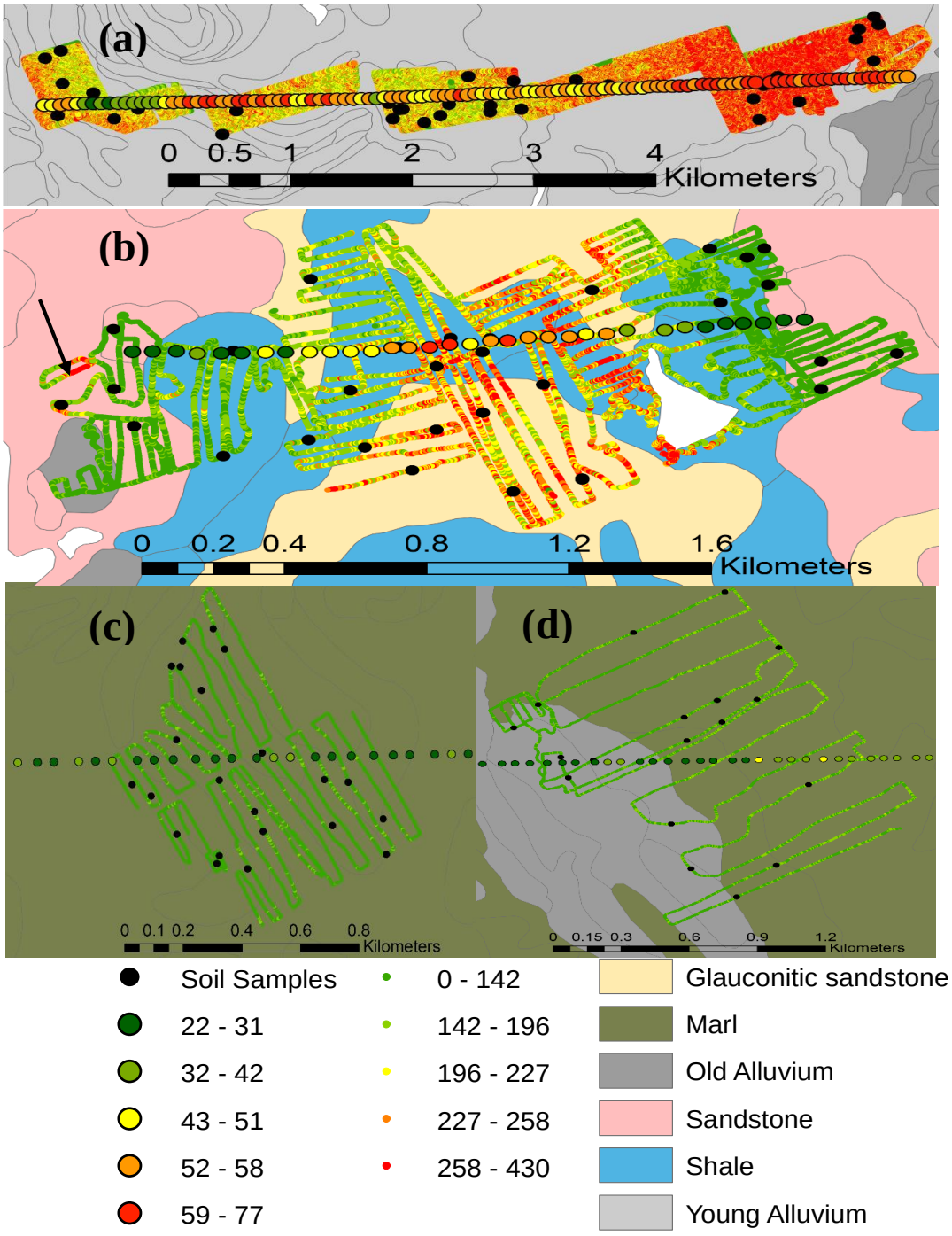

Figure 11. Gamma radiometric sites a) A, b) B, and c) C1 and d) C2. Each site has the aerial (larger colored circles) and proximal (smaller colored circles) dose rate (Bq kg^{-1}) with generalized bedrock types according to county soil surveys. Soil sampling locations are marked with black dots. The white polygon at site B represents a local water body.

III.2.2. Aerial Gamma Radiometric Surveys

The aerial gamma radiometric surveys within each of the sites were conducted at different times and dates, as well as from different contractors. All sites were surveyed for the National Uranium Resource Evaluation program. Sites A and B were conducted by Geodata International, Inc. on April 20 and 21, 1977, respectively. Sites A and B lie along different transect lines (Geodata International Inc., 1979; Hill et al., 2009). The Site C survey was conducted by EG&G Geometrics, Inc. on October 11, 1979 (Geometrics, 1980; Hill et al., 2009).

The survey for Sites A and B used nine NaI scintillation crystals. Eight crystals of 55.5 L were directed downward (4π steradian solid angle) and one 6.8 L crystal was directed upward (2π steradian solid angle). The flight was standardized to an altitude of 120 m, and the average along-line distances for Sites A and B are 65 and 63 m, respectively. The average altitudes are 131 and 124 meters, respectively.

Spectral information was collected by a pulse height analyzer every second and stored onto magnetic tape (Geodata International Inc., 1979). During post-processing, the downward looking crystal spectral data were converted into elemental concentrations using the following energy windows: ^{40}K (1.322 MeV-1.638 MeV); ^{238}eU (1.05-1.322 plus 1.638-2.410 MeV); ^{232}eTh (2.41 to 2.796 MeV). The data were then corrected for atmospheric radiation and altitude effects and converted to concentrations using experimentally determined sensitivity coefficients (Geodata International Inc., 1979; Minty, 1997a; IAEA, 2003).

Positional information was determined relative to a base point and heading using a combination of radar altimeter and a Doppler navigation system in a technique called dead-reckoning, which determines position based on velocity measurements (Kayton and Fried, 1997). During the survey, a co-pilot would write the record numbers or fiducials associated with visual check points such as cross roads or rivers, and these record numbers would be used as input to flight path recovery (Geodata International Inc., 1979). These pick-points serve as the basis for which all other sample points are geo-referenced, as spectral measurements were not instantaneously coupled with positional information.

The geo-spatial accuracies of the aerial point measurements were checked using the surficial geology code assigned to each point along the transect line (Hill et al., 2009). This analysis revealed that gamma points located in Site A contained points with residuum geology codes, rather than alluvium, indicating a positional error. A positional error was also present at Site B, although its effects were less apparent because the soils formed under the same landform (i.e. uplands) rather than an abrupt transition (i.e. young alluvium to old alluvium) (Fig. 11). To remedy the positional offset of the aerial point measurements at Sites A and B, the surveys in Sites A and B were shifted along their respective transect lines based on the geomorphology of the surrounding areas as well as the direction of the aircraft during data collection. For example at Site A, aerial points were shifted approximately 1200 m east, toward sandier more weathered terrace material. Soils that develop over terraces were expected to emit a relatively lower amount of gamma radiation due to a higher degree of soil development (Wilford et al.,

1997). The positional shift applied to Site B was more complicated because neither abrupt geomorphic features nor large bodies of water were present (Ahl et al., 2014). A shift of approximately 250 m east was applied based on the presence of forested areas. High wood content can attenuate gamma-rays because it contains an electron density higher than that found in soil (Wetterlind et al., 2012).

Similar to surveys at Sites A and B, EG&G Geometrics, Inc. used a standardized flight sensor altitude of 120 m collected at one-second intervals (Geometrics, 1980). Geometrics used 50.3 and 8.4 L of NaI scintillation crystals for downward and upward looking directions, respectively. The system was also mounted on a fixed wing aircraft traveling at a general velocity of 225 km hr^{-1}. The average along-line distance in the study area is 68 m, and the average altitude is 114 m.

The spectral data collection methodology was similar to that of Sites A and B in terms of sampling interval, but the spectral energy window ranges differed as follows: ^{40}K (1.37 to 1.57 MeV); ^{238}eU (1.04 to 1.21 plus 1.65 to 2.42 MeV) and ^{232}eTh (2.41 to 2.81 MeV). The flight path recovery technique was also different from Sites A and B, as a 35 mm tracking camera with a fiducial numbering system was used that instantaneously joined all spectral and positional data based on common fiducial numbers (Geometrics, 1980). The information content within the metadata for Site C differed from Sites A and B, as the former was more detailed in its processing steps. As well, coefficients for altitude were calculated, which is particularly useful if error budgets are to be created for legacy aerial gamma radiometric data (Løvborg and Mose, 1987).

III.2.3. Proximal Gamma Radiometric Surveys

The proximal gamma radiometric data were collected from a 4 L volume NaI gamma-ray spectrometer (Radiation Solutions Inc., Mississauga, Ontario, Canada). A mounting device for the spectrometer was installed onto the passenger side of a John Deere Gator field vehicle, with the sensor located at a height of approximately 55 cm above the ground.

The line spacing distances were not constant for all sites - the maximum line spacing distance was approximately 50 m (Site C2), while the lowest was 20 m (Site B). The speed of the vehicle across all Sites was consistent, approximately 4.5 m s^{-1}. Raw continuous spectral data was collected every second in the form of ^{40}K, ^{238}U and ^{232}Th mass concentrations that were instantaneously joined with spatially referenced coordinates collected by a Wide Area Augmentation System (WAAS) enabled GPS unit. The radioelement energy windows for the sensor are as follows, ^{40}K (1.37 to 1.57 MeV); ^{238}eU (1.66 to 1.86 MeV), and ^{232}eTh (2.41 to 2.81 MeV) (Radiation Solutions Inc.).

Soil sampling design for Sites A and C1 was stratified using topography and aerial imagery. For Sites B and C2 the proximal gamma radiometric survey was stratified and randomly sampled. Soil samples were then collected at 0 to 15 cm depths. After proximal surveys were concluded, 34, 37, 24, and 19, soil samples were collected at Sites A, B, C1, and C2 respectively.

Soil samples were air dried to 60°C for 48 hours and ground to pass through a 2-mm sieve. Soil particle-size distribution for all samples were measured using the pipette

method and wet-sieving sands (Gee and Or, 2002). Soil texture classes were assigned using the USDA soil textural classification system, and their distribution is shown in Figure 12. Inorganic carbon was only measured at Sites C1 and C2 because the soils effervesced when 10 N HCl was applied. Inorganic carbon was measured using the modified-pressure calcimeter method (Sherrod et al., 2002). Inorganic carbon mass concentrations (g kg^{-1}) were then converted into calcium carbonate equivalent by dividing by the inorganic carbon concentration by the molecular weight fraction of carbon (0.12).

The laboratory information was then imported and managed alongside the proximal and aerial gamma spectral data within R (R Development Core Team, 2014). Descriptive statistics for gamma-ray variables (^{40}K, ^{238}eU and ^{232}Th) as well as laboratory derived soil properties are shown in Table 6. The standard output provided by both the proximal and aerial sensor data (parts per million) were converted into specific activity (Bq kg^{-1}) using constants defined by IAEA (2003).

Table 6: Descriptive statistics of soil sample analysis with proximal (P) and aerial (A) gamma radiometrics collected within each site. Dose rate is in nGy hr^{-1}, while ^{40}K, ^{238}U and ^{232}Th are in Bq kg^{-1}.

	Min.	**Max.**	**Std. dev.**	**Mean**
			Site A	
Soil properties, g kg^{-1}				
Clay	91	733	236	362
Sand	8	648	189	181
Silt	188	698	150	457
Gamma radiometrics				
Dose Rate (P)	72	328	37	232
^{40}K (P)	281	3167	369	2187
^{238}U (P)	36.5	301	34	142
^{232}Th (P)	13	202	27	115
Dose rate (A)	28	76	8	54
^{40}K (A)	0.5	2.3	0.3	1.48
^{238}U (A)	0.5	3.9	0.7	2.19
^{232}Th (A)	2.9	13.1	2.0	8.29
			Site B	
Soil properties, g kg^{-1}				
Clay	11	484	145	212
Sand	290	932	210	584
Silt	54	433	82	203
Gamma radiometrics				
Dose rate (P)	60	401	52	177
^{40}K (P)	130	2446	432	982
^{238}U (P)	28	388	29	118
^{232}Th (P)	13.6	314	51	124
Dose Rate (A)	28	73	14	51
^{40}K (A)	0.1	1.7	0.4	0.71
^{238}U (A)	0.9	3.7	0.6	1.92
^{232}Th (A)	4.6	17.8	3.8	11.3
			Site C1	
Soil Properties, g kg^{-1}				
Clay	399	553	37	488
Sand	84	189	25	131
Silt	326	467	33	382

Table 6 Continued	**Min.**	**Max.**	**Std. dev.**	**Mean**
Calcium carbonate equivalent	146	486	103	288
Gamma Radiometrics				
Dose rate (P)	55	147	13	106
^{40}K (P)	148	930	110	520
^{238}U (P)	0	123	17	57
^{232}Th (P)	31	148	19	87
Dose rate (A)	48	52	1	33
^{40}K (A)	0.5	0.6	0.0	0.53
^{238}U (A)	0.9	1.5	0.2	1.21
^{232}Th (A)	6.8	7.7	0.3	7.3
			Site C2	
Soil properties, g kg^{-1}				
Clay	180	554	102	424
Sand	69	454	108	186
Silt	340	450	31	389
Calcium carbonate equivalent	0	17	4	2
Gamma radiometrics				
Dose rate (P)	44	169	23	125
^{40}K (P)	51	1165	197	570
^{238}U (P)	12	165	19.9	75
^{232}Th (P)	12	171	23.4	101
Dose rate (A)	33	46	4	41
^{40}K (A)	0.5	0.8	0.1	0.63
^{238}U (A)	1.4	2.4	0.3	1.92
^{232}Th (A)	6.7	9.3	0.7	8.02

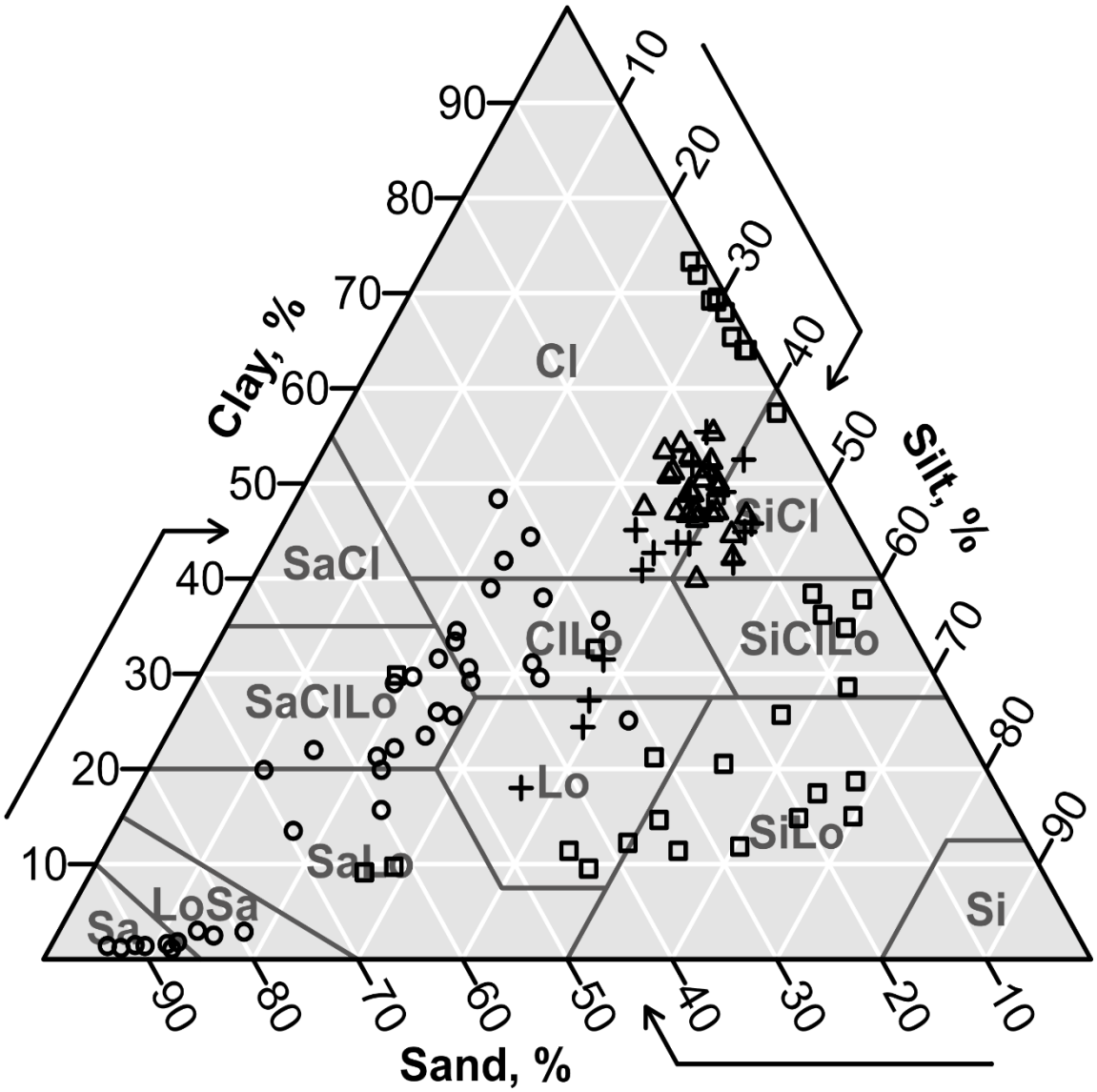

Figure 12. A summary of soil texture classes for each site on a United States Department of Agriculture soil textural triangle. Sites A, B, C1 and C2 are represented by squares, circles, triangles and crosses, respectively. Reprinted from R code provided by Moeys (2015), originally sourced from Soil Survey Staff (1993).

III.2.4. Data Management and Statistical Modeling

Prior to merging soil property data with proximal gamma radiometrics, the latter was smoothed and interpolated. To increase the signal-noise ratio, a spatial moving average

of five measurements was calculated as suggested by Viscarra-Rossel et al. (2014). Additionally, proximal radiometric values that were outside of two standard deviations of the five-point averaged data were removed. Proximal radiometric data were then interpolated using inverse distance weighting, in the gstat package in R.

Pearson correlation coefficients and their significance between laboratory soil properties and proximal gamma radiometrics were calculated. Under the assumption that soil moisture influences gamma spectral measurements signal, equation 1.5 was applied using a soil moisture measured at the time of the proximal gamma radiometrics measurements. Pearson correlation coefficients were reassessed (Appendix B). The results after moisture correction did not improve the Pearson correlation coefficients, and all models were therefore based off non-corrected proximal gamma radiometrics data – a similar result was found by Priori et al. (2014).

The proximal gamma radiometric variables (^{40}K, ^{238}eU and ^{232}Th) were then related to soil texture and calcium carbonate equivalent within and across all Sites through Pearson correlation coefficients and linear regression modeling. First simple regression models between each soil property and ^{40}K, ^{238}U and ^{232}Th (including dose rate) were created. To test the hypothesis that the GR signal is parent material specific, the estimated slope coefficients and intercepts describing the relationship between soil properties and proximal radiometric data between each site were compared using analysis of covariance (ANCOVA). Second, multiple linear regression models were fit using all three variables as predictors, with their removal contingent on an inflation factor (VIF) greater than or equal to 5, as the variables can exhibit multi-collinearity

(Rodrigues Jr. et al., 2015). Stepwise-backwards elimination regression was then performed for the ^{40}K, ^{238}U and ^{232}Th predictors, eliminating variables that were insignificant (p-value ≥ 0.05). The goodness-of-fit measures used to assess the models were the adjusted coefficient of determination (Adj. R^2), as well as root-mean squared error (RMSE) and residual plots.

Aerial gamma radiometric transect point data were compared with proximal gamma radiometric data through footprint analysis (Fig. 11). For each aerial gamma radiometric transect point, ellipsoidal buffers of size 265 and 378 m in the across-track and along-directions, respectively, were created for every aerial gamma point measurement (Kosanke and Koch, 1978; Pitkin and Duval, 1980; Beamish, 2013). All of the proximal gamma radiometric values located within each buffer were averaged within an inverse-distance weight to the ellipsoid center because the most intense signal is found directly beneath the detector (Kock and Samuelsson, 2011; Beamish, 2014). Scatter plots that relate aerial gamma radiometrics with spatially-averaged proximal gamma radiometrics were created and assessed by conducting an ANCOVA.

III.3. Results and Discussion

III.3.1. Proximal Gamma Radiometric Surveys

Proximal and aerial gamma radiometric data were both spatially variable, both within and across parent materials (Fig. 11). In general, soils forming in alluvium in Site A and glauconitic sandstone in Site B (high ^{40}K) emit higher amounts of gamma radiation than that from the siliceous sandstones (Site B), while the marl residuum found in Sites C1 and C2 was lowest in radioelemental abundance (Figs. 11a-11c). Limestone-

based rocks such as marl are generally known to contain low amounts of radioelement concentrations due to an absence of gamma-rich silicates and abundance in carbonates (Ford et al., 2008; Stahr et al., 2013).

A particularly interesting proximal gamma radiometric feature can be seen at the west end of Site B (Fig. 11b, arrow), where a pocket of unexpectedly high gamma radiation is present due to erosion of the sandy A and E horizons from local stream entrenchment, leaving behind an exposed clay-rich horizon. In addition to erosional features, the proximal sensor is also able to detect the presence of non-soil components at a high resolution such as roads (low gamma radiation, green) in Site A that are highly contrasted with nearby gamma-rich alluvial clay soils eastward (Fig. 11a).

III.3.2. Proximal Gamma Radiometric and Soil Correlation Results

The Pearson correlation analyses between proximal gamma radiometrics and laboratory soil properties are shown in Table 7. At Sites A and C2, dose rate has the strongest correlation with soil properties, with ^{232}Th being equal or weaker than dose rate. At Site B, ^{232}Th correlation with soil particle size was stronger than dose rate. In general, ^{238}U was not correlated with soil properties. The particular soil property with the highest correlation varied by Site and was not consistent. For example, clay content correlation in Site A was much greater than that for Site B, while the opposite was true for sand content (Table 7). The relative age of the soils at these Sites might explain this observation, as there has not been a sufficient amount of time for ^{40}K to become solubilized and lost from the soil surface at Site A (Wilford et al., 1997).

Although previous research (Buchanan et al., 2012) has suggested that silt content, unlike clay and sand content, is less well correlated with proximal gamma radiometrics data due to its mixture of quartz and secondary minerals, the magnitude of correlation for silt content was higher than sand at Site A (Table 7). Such strong relationships with silt likely occurred because of its negative co-correlation with clay content ($\rho = -0.61$). Therefore, the relationship between silt content and proximal gamma radiometrics measurements are only reliable to the extent that clay and/or sand content are correlated with silt. The signs of the correlation coefficients for clay are consistently positive and sand content consistently negative, while the signs for silt content varied. This variation of positive and negative correlations with silt maybe attributed to the original source mineralogy that may or may not have undergone weathering to smaller particle sizes (Bierwirth, 1996).

In terms of individual proximal gamma radiometric variables, the ^{40}K and ^{232}Th radioelements provided the more consistent and stronger models across all properties and Sites, while ^{238}U was only weakly correlated at Site A (Table 7). ^{232}Th is highly retained onto clay surfaces, and although it can become solubilized in very acidic conditions or adsorbed by organic complexes, this does not appear to be the case here (Bierwirth et al., 1996; Rachkova et al., 2010; Wilford, 2012). At Site B, the listed mineralogy types in the area (mixed, siliceous, smectitic) were more sharply contrasting in ^{40}K and ^{232}Th and less contrasting than ^{238}U. Though ^{238}U has the highest coefficient of variation of all proximal gamma radiometric variables, it has the least amount of info on measured soil properties.

Table 7: Significant Pearson correlation coefficients (p-value < 0.05) between proximal gamma radiometric measurements and lab-characterized soil data.

Soil property	Dose Rate	^{40}K	^{238}U	^{232}Th
		Site A		
Clay	0.90	0.91	0.58	0.87
Sand	-0.54	-0.60	NS	-0.53
Silt	-0.74	-0.67	-0.56	-0.70
		Site B		
Clay	0.74	0.64	NS	0.79
Sand	-0.77	-0.66	NS	-0.83
Silt	0.68	0.55	NS	0.73
		Site C1		
Clay	NS	NS	NS	NS
Sand	NS	NS	NS	NS
Silt	NS	NS	NS	-0.43
Calcium Carbonate	-0.71	NS	NS	-0.71
		Site C2		
Clay	0.91	0.70	NS	0.66
Sand	-0.93	-0.76	NS	-0.70
Silt	NS	NS	NS	NS
Calcium Carbonate	NS	NS	NS	NS

In addition to comparing soil properties and ^{40}K, ^{238}U and ^{232}Th variables, correlations with dose rate (more representative of the entire gamma-ray spectrum) was also done. There are conflicting conclusions regarding whether ^{40}K, ^{238}U and ^{232}Th or dose rate provides more information on spatial variation of soil properties (Mahmood et al., 2013). In general, dose rate and soil property relationships had smaller correlation coefficients compared to ^{232}Th, although dose rate in Site C2 outperformed the individual windows due to strong relationships with ^{40}K (Table 7). Using dose rate over the individual energy windows is therefore contingent upon the spatial variability of not

only ^{232}Th, but ^{40}K as well (Bierwirth, 1996). An additional representation of the gamma-ray spectrum includes full-spectrum analysis, but such a technique was not implemented in this study because the legacy aerial gamma radiometrics only provide specific energy windows and not full spectra information.

III.3.3. Models of Soil Properties Using Proximal Gamma Radiometric Data

III.3.3.1. Texture

The magnitude of adjusted r-squared (Adj. R^2) between the individual soil texture components and proximal gamma radiometric data differs by Site, although areas that are alluvium-derived (i.e. Sites A, C2) generally had higher Adj. R^2 than soils developed from residuum (Table 8). Sites B and C2 contained the most statistically significant linear models between soil and proximal gamma radiometric variables (Table 8). Relationships between sand content and proximal data at site A were not linear because the soils high in sands have not been sufficiently weathered, and thus contain higher than expected gamma signatures. Site C1 performed poorly with proximal gamma radiometrics because the surface textures were predominantly clay (Table 8 and Figure 11c). Site C2 also contains high clay textured soils forming from marl, but unlike Site C1 it contains Alfisols forming from old alluvium. Hence, Site C2 has more significant models for clay and sand content because of the translocation of silicate clays.

Table 8: Linear Regression models within and between sites and Analysis of Covariance (ANCOVA) results between sites.

Site	Adj. R^2	Model	RMSE†	Sites Compared	Sign. Diff. † S.	I.
			g kg^{-1}			
		Clay				
All	0.19	357.1+0.1*K-3.3*U+1.8*Th	168	-		
A	0.85	-1708.2+0.8*K+4.9*Th	144	N/A	N/A	N/A
B	0.40	-22.2+0.2*K	117	B to A	N	Y
C2	0.82	-539.4+0.2*K+4.1*U+5.1*Th	38	C2 to A	Y	Y
		Sand				
All	0.33	10.1-0.009K+0.16*U	303	-	-	-
A*	0.68	14.66-0.005*K	170	N/A	N/A	N/A
B	0.42	932.2-0.4*K	163	B to A	N	N
C2	0.85	1170.7-0.3*K-3.6*U-5.4*Th	50	C2 to A	N	N
		Calcium carbonate equivalent				
C1+ C2	0.67	1149.1-5.9*U-6.3*Th	90	-	-	-
C1	0.48	857.7-6.4*Th	80	C1 to C2	Y	Y

†RMSE is Root Mean Squared Error; S is slope and I is intercept.
* Model was log-(Y) and square-root(X) transformed.

The lower Adj. R^2 at Site B relative to Sites A and C2 is attributed to the soils being in a more advanced stage of weathering. Weathering of soil minerals and translocation of clay-sized particles is advanced and maybe used to explain the scatter from the line of best fit for Site B (Fig. 13). For example, an outlier point (oval labeled 'I') that has a low dose rate due to ^{40}K abundance could be due to the natural weathering or alteration of glauconite into secondary clay minerals such as vermiculite or montmorillonite, that are clay-sized particles. During this process, ^{40}K is lost from its structure (McRae, 1972). One key indicator (besides mineralogical data) that was used to formulate this hypothesis was the observation of iron oxidation commonly associated with glauconitic

weathering, at this particular sample point (McRae, 1972). Additional points ('II') could also be explained in terms of glauconite weathering, whereby a relatively low amount of ^{232}Th was measured due to its co-precipitation with iron in the sand-sized fraction (Rachkova et al., 2010). Visual analysis confirmed the mobility of iron hydroxides in subsurface samples.

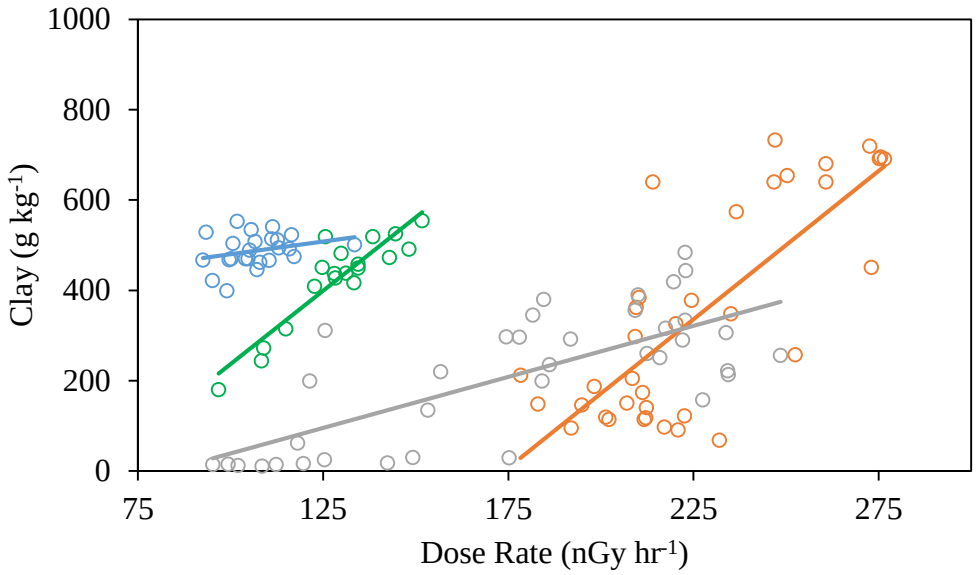

Figure 13. Proximal gamma radiometrics (dose rate) by site plotted with measured clay content, where Sites A, B, C1 and C2 are indicated by orange, grey, blue and green circles, respectively.

In addition to soil mineralogy, the scatter plot for clay content at Site B could be influenced by the relative location of the soil sample along a given catena. Figure 11b shows that Site B contains sample points that contain higher than expected radiometric values at low clay content and this is most likely due to their location on back slopes

(ranging from 2 to 8 percent), thereby the underlying Bt horizons are nearer to the surface; the most extreme example can be found in Figure 11 (III), and this point coincides with the sample located nearest the high pocket of gamma radiation (section III.3.1). In addition to clay content, sand content and proximal gamma relationships were strong and in general linear except for site A which can most likely explained through the predominance of gamma-rich sources within the sand and/or silt fractions (Fig. 14).

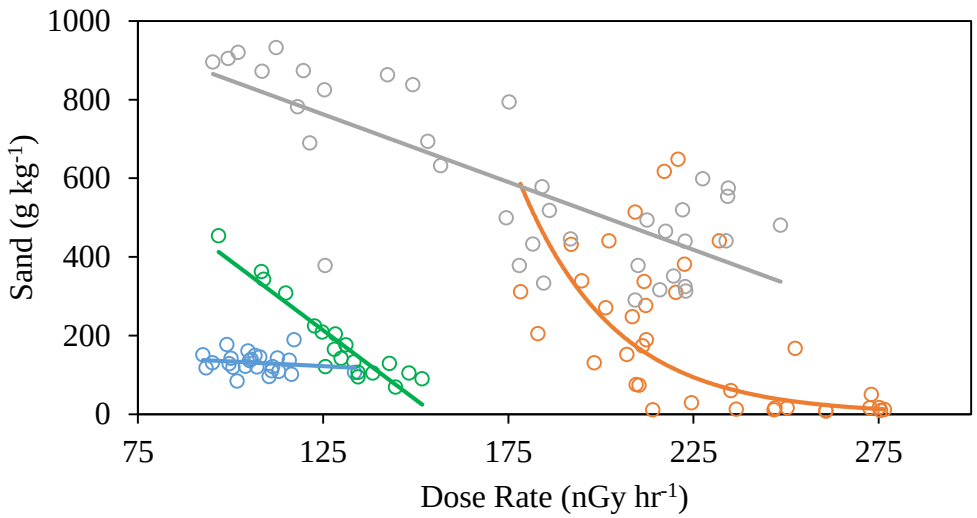

Figure 14. Proximal gamma radiometrics (dose rate) by site plotted with measured sand content, where Sites A, B, C1 and C2 are indicated by orange, grey, blue and green circles, respectively.

III.3.3.2. Calcium Carbonate Equivalent

Although the relationship between texture and proximal gamma radiometrics was poor within Site C1, the model for calcium carbonate equivalent and proximal gamma radiometrics was strong (Fig. 15). These soils are high in clay (all over 400 g kg^{-1}) and

weathered from marls and chalks rich in calcium carbonate. ^{232}Th is clearly the radioelement that is responding the carbonate concentrations, not ^{40}K. While ^{232}Th and exhibit similar patterns due to their adsorption onto clay minerals, preferential loss of ^{40}K (and retention of ^{232}Th) can occur when soils are subjected to fluid migration as several samples were located near an old fluvial channel.

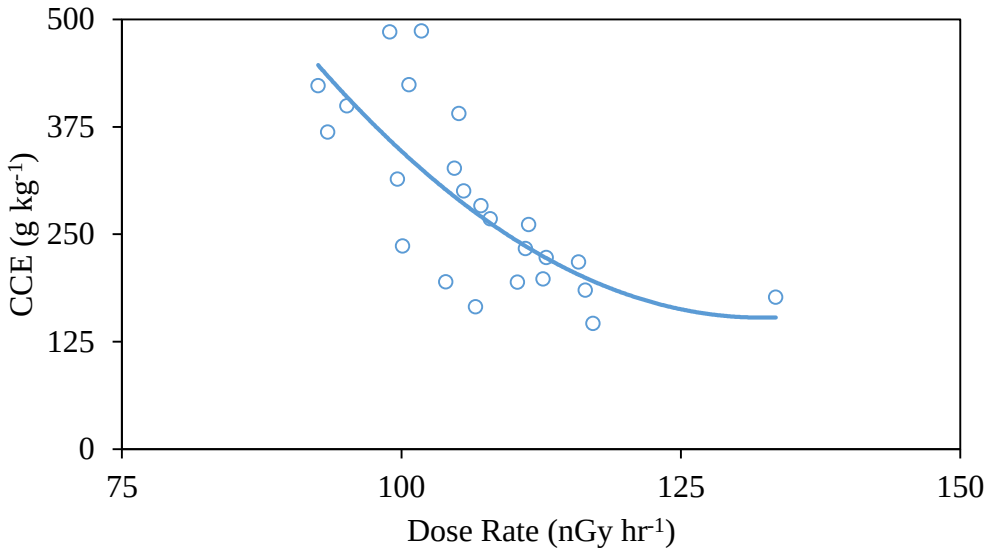

Figure 15. Proximal gamma radiometrics (dose rate) by site plotted with measured calcium carbonate equivalent (CCE) , where Sites A, B, C1 and C2 are indicated by orange, grey, blue and green circles, respectively.

In summary, proximal gamma radiometric measurements are most successful in mapping soil texture and calcium carbonate content only when the soil properties are variable themselves, a feature of which is a function of parent material type, weathering history, and localized soil conditions.

III.3.3.3. Site-specific Tests

When soil measurements from all sites and their proximal gamma radiometric data are combined into one model, the Adj. R^2 values are much lower, and the RMSE values were higher than the site-specific RMSE models (Table 8). The overall Adj. R^2 clay models were much lower than that of sand and silt content, indicating that proximal gamma radiometric predictions of clay content are more sensitive to site-specific conditions (Mahmood et al., 2013). In comparing models between sites using ANCOVA models, the intercept and slope estimates from Sites A and B models were uniquely different from each other as well as Sites C1 and C2 (Table 8).

III.3.4. Proximal and Aerial Gamma Radiometric Comparative Analysis

Comparison of aerial with proximal gamma radiometrics allows some assessment of the quality and reliability of the legacy aerial gamma radiometric data. Scatter plots and linear trends between aerial and proximal gamma radiometric variables such as ^{40}K, ^{238}U and ^{232}Th and dose rate were assessed (Fig. 16).

Site A generally has higher radiometric concentrations than Sites B and C, and this is attributed to the 'fresh' radiometric deposits delivered by the Brazos River within the last 2000 years (Biewirth, 1996; Chervenka, 2002) (Fig. 16). The one exception to this generalization is for ^{232}Th at Site B, where soils formed from a marine shale rich in glauconite, which is associated with highly elevated ^{232}Th abundances (Gunn et al., 1997; Wilford et al., 2015) (Fig. 16d). The lowest radiometric abundances occurred at Site C, as these soils developed from sedimentary carbonates (Ford et al., 2008; Wilford et al., 2012).

Aerial versus proximal gamma radiometrics at each site are generally in good agreement with each other, indicating that aerial data are adequately representing the spatial patterns on the ground, even within highly variable landforms such as at Site C (i.e. upland residuum grading into terraces, Fig. 16). Aerial gamma radiometrics at Site A, however, is most poorly related with proximal variables. The correlation was worse before spatially shifting the aerial data; however, the aerial data still appears poorly geo-located because of the poor match with the proximal survey.

If aerial gamma radiometric data is to be used seamlessly as a soil property covariate across a physiographic region, a repeatable response between aerial and proximal gamma radiometrics is needed. While the intercept of a regression line between aerial proximal gamma radiometrics might change due to base line abundances of ^{40}K, ^{238}U and ^{232}Th in a soil, a consistent slope between parent material sites would show a similar GR response to soil properties between aerial and proximal surveys. An ANCOVA analysis was used to test this response by comparing the slopes and intercepts of the regression lines of aerial and proximal gamma radiometrics between sites (Table 9).

Among the main radioelements (^{40}K, ^{238}U, ^{232}Th) ^{40}K provided the most consistent and strongest relationship between aerial and proximal gamma radiometrics across all sites. Additionally, the ^{40}K model resulting from the combination of all sites is an improved model compared to individual Sites A and B (Table 9). ^{40}K likely achieved better correlations between aerial and proximal gamma radiometrics compared with the other ^{40}K, ^{238}U and ^{232}Th and dose rate because of the higher count rates encountered within its window, thus creating a higher signal to noise ratio. The fractional

measurement of gamma radiation operates under the Poisson distribution ($\frac{\sigma(n)}{n} = \sqrt{\frac{1}{nt}}$, where nt = total counts per unit time) (IAEA, 2003). It should be noted that the above equation applies to gamma measurements on a count basis rather than a concentration basis; however, the conversion is linear and the trends do not change.

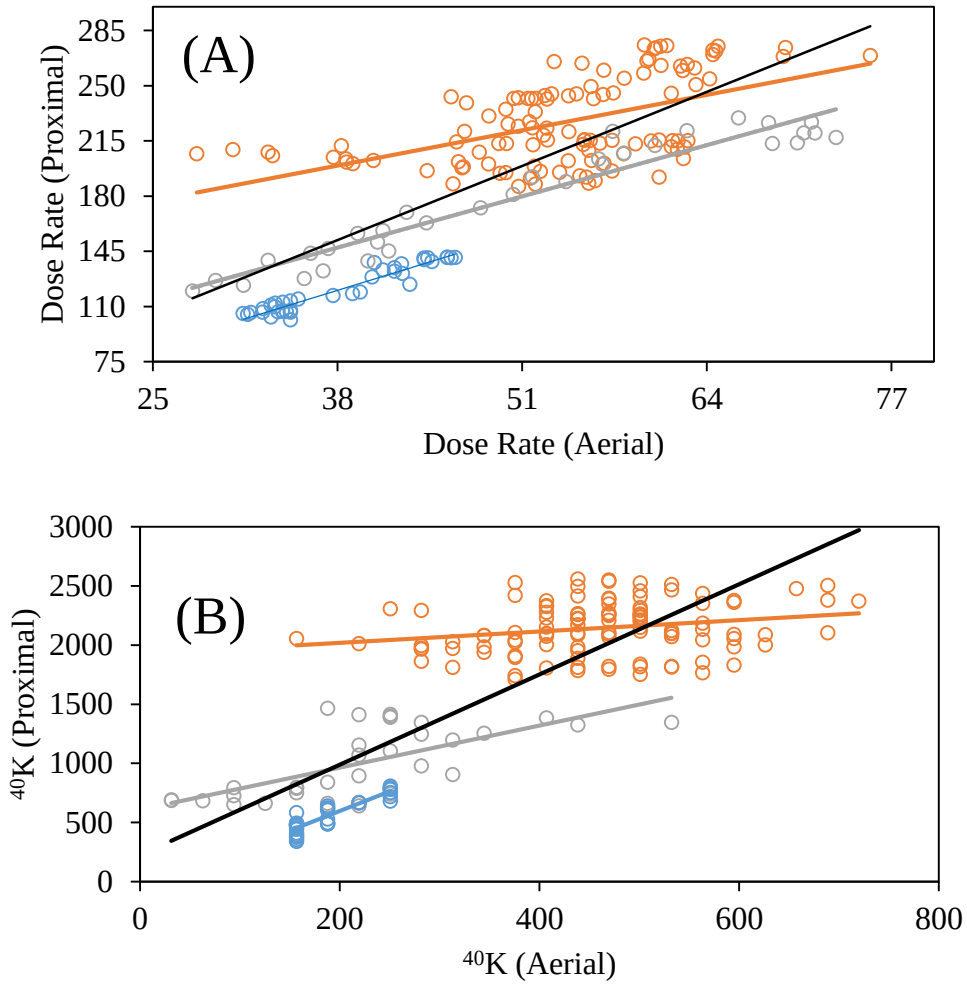

Figure 16. Proximal plotted versus aerial gamma radiometrics for a) dose rate, b) ^{40}K; c) ^{238}U, and d) ^{232}Th. Sites A, B and C are indicated by red, black, and blue circles, respectively.

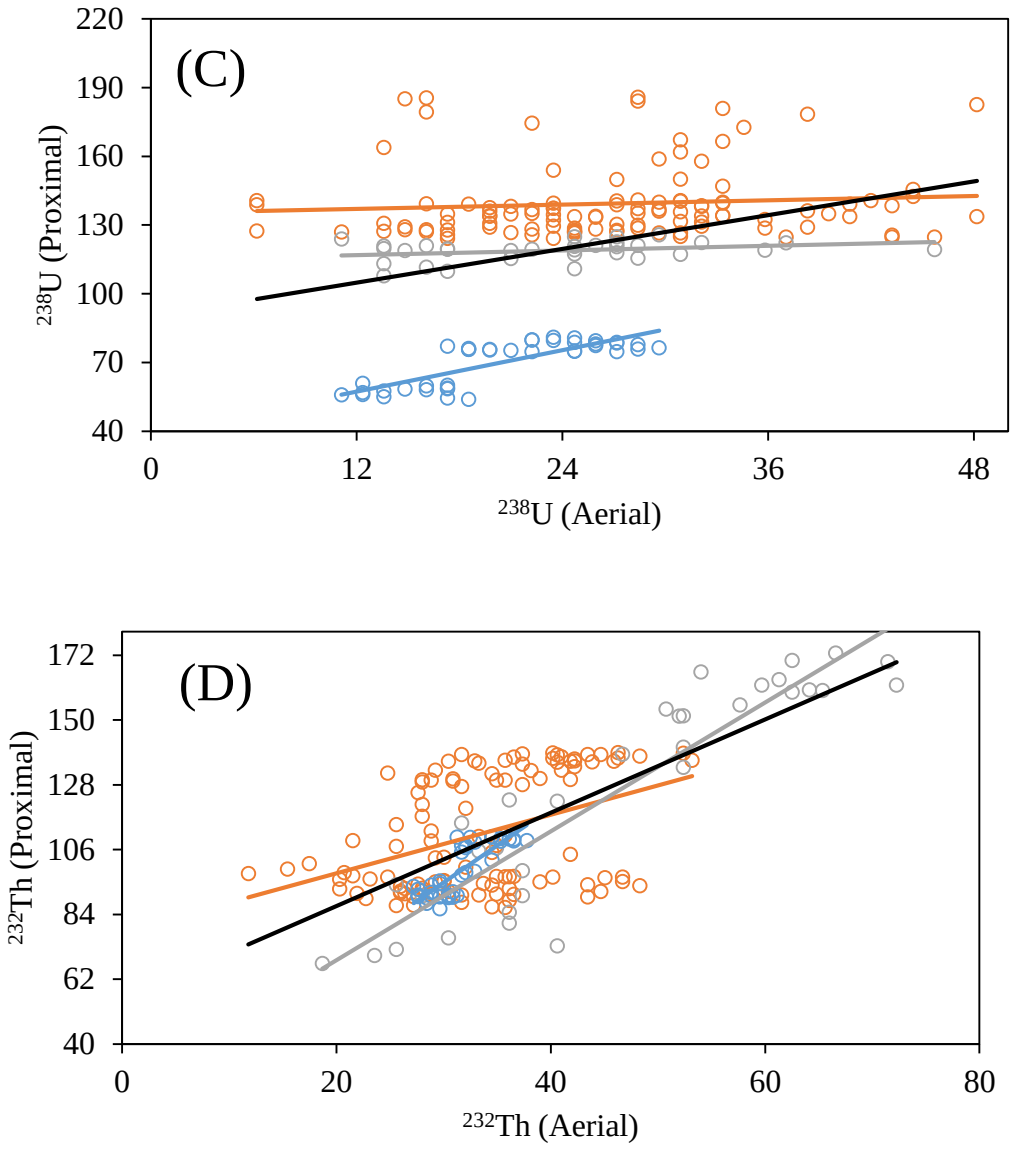

Figure 16. Continued.

Table 9: Linear regression R^2 values comparing aerial and proximal gamma radiometric measurements are shown. As well, Analysis of Covariance (ANCOVA) results comparing slopes and intercepts to of each regression model to Site B when Site B is significant (p value ≤ 0.001).

Site	N	R^2	Sites Compared	Significantly Different	
				Slope	Intercept
			Dose Rate		
All Sites	183	0.61	-	-	-
A	111	0.26	A to B	N	Y
B	33	0.93	-	-	-
C	39	0.90	C to B	N	N
			^{40}K		
All Sites	183	0.69	-	-	-
A	111	NS	-	-	-
B	33	0.43	-	-	-
C	39	0.78	C to B	N	Y
			^{238}U		
All Sites	183	0.11	-	-	-
A	111	NS			
B	33	NS	-	-	-
C	39	0.62	-	-	-
			^{232}Th		
All Sites	183	0.49	-	-	-
A	111	0.16	A to B	Y	Y
B	33	0.84	-	-	-
C	39	0.68	C to B	N	N

Overall, the ^{232}Th and ^{40}K responses between aerial and proximal gamma radiometrics is quite similar between Sites C and B. The response at Site A is weak to begin with and might be similar if the positioning were better. The slopes of dose rate were similar between Sites, while the intercept is much higher for floodplains (Site A). Again, it is not clear if this is an effect of poor geo-referencing of the aerial gamma radiometric data.

^{238}U is the only model that contains weak and no-significant comparisons between aerial and proximal gamma radiometrics that can be attributed to differences in soil moisture, differences in radon, a daughter product of ^{238}U due to changing temperatures and pressures, and low counting measurements, or low signal-to-noise ratio (Bierwirth, 1996; Minty, 1997a; Dickson, 2004). Analysis of historical weather data indicates that a rain event did occur before the time of the aerial gamma radiometric surveys at Sites A and B (not at C). Ideally, aerial gamma radiometric surveys should be supplemented by soil moisture data (Carroll, 1981), but the aerial gamma radiometric surveys were conducted only once, and the influence of soil moisture on the aerial ^{238}U cannot be assessed (Beamish, 2015).

The FOV that was selected for this analysis was based on the height and movement of the sensor, but such estimations are theoretical in nature, a problem that is further compounded when different sensor configurations are considered (Billings and Hovgaard, 1999). One source of error that could explain noise between aerial and proximal gamma radiometrics could be gamma-rays measured outside the FOV, but this feature is usually not a problem because the change in correlation between aerial and proximal gamma radiometric measurements begins to level off with increasing FOV size (Kock and Samuelsson, 2011). An additional source of error could lie within the representation of the FOV. While others have identified an optimal FOV size based on the highest R^2 (Bollhoffer et al., 2013), this analysis used approximations actual conditions based on theory (Billings and Hovgaard, 1999). Although with the two methods measuring different areas, inaccurate positioning is suspected to be the main

driver of differences between aerial and proximal gamma radiometrics, as well as the spectral energy ranges measured are not identical. These results suggest that the overall aerial and proximal gamma radiometric comparisons can be successful, given that the initial point positions are accurately marked.

III.3.5. Spatial Shifting of Aerial Gamma Radiometric Point Data

Although the US aerial gamma data from the 1970s will always be associated with a certain amount of positional uncertainty, there are general guidelines that can be used to check the positional accuracy of a given aerial gamma radiometric survey. First, aerial gamma radiometric measurements over large bodies of water are expected to provide a significantly lower gamma signature than any soil body (Ahl et al., 2014). Second, aerial gamma radiometric measurements over areas that abruptly change in geomorphology generally correspond with abrupt changes in gamma emissions (Wilford et al., 1997). Third, areas that are heavily forested with a high wood density also provide an indicator of gamma-ray attenuation, as these types of vegetation can hold large volumes of water (Wetterlind et al., 2012). Unfortunately, the Sites in this study did not contain a nearby large (i.e. greater than the FOV) body of water, and so we used the second and third methods for Sites A and B, respectively.

As explained previously, aerial gamma radiometrics at Site A seemed to provide the most disagreement with proximal gamma radiometrics after spatial shifts were applied (Fig. 16). The source of geo-spatial inaccuracy in modern aerial gamma radiometric systems stems from many inevitable sources, such as: 1) timing errors between the measurement and recording events; and 2) instantaneous precision of a non-differential

GPS system (Cardarelli II et al., 2011; Ahl et al., 2014). Not all of the above sources are applicable to the legacy US aerial gamma radiometric survey, as GPS was not implemented and instead a Doppler radar system was used. When all of these sources of error are combined, Cardarelli II et al. (2011) stated that the theoretical maximum shift would be 130 m in the direction of travel. However, the aerial survey conducted over Sites A and B required 1140 and 240 m.

Further investigation into the metadata provided by Geodata International, Inc. revealed that potential sources of error lie within the transfer of positional information originally stored on the magnetic tape. We first considered Doppler radar error as the source; however, the shift applied was found to be systematic, meaning that the amount of shift needed did not change along-line, thus eliminating Doppler radar as a significant source of error (Kayton and Fried, 1997).

Because the spatial shifts for Sites A and B varied, we suspect that the positional error is mainly attributed to the flight path recovery methodology used by Geodata International, Inc. Only pick-point records were selected based on landmark features, which were then identified on a base map - it is possible that the copilot or navigator responsible for marking these records either mislabeled the record number with the visual check point, or did not correctly associate the visual check-point with the reference information on the base map. Regardless of the source of the positional errors, the errors will regardless contribute to uncertainty when trying to use aerial gamma radiometrics as a covariate to map soil data.

III.4. Conclusions

Relationships between soil properties such as clay, sand and calcium carbonate and their associated proximal gamma radiometric measurements correlate strongly, although the soil property with the strongest correlations varied by site. The trends for clay and sand content with dose rate and ^{40}K, ^{238}U and ^{232}Th were positive and negative, respectively, whereas the trend was ambiguous. The highest correlations (0.91 and -0.93 for clay and sand content, respectively) were located under a geomorphically diverse area with differential rates of pedogenesis and on old and new alluvium parent material. The gamma energy windows that exhibited the overall highest correlations with soil properties were (in order): ^{232}Th, ^{40}K and ^{238}U, although ^{40}K had strongest correlations with clay and sand in residuum/alluvium combinations. ^{238}U had a low signal to noise ratio and was generally poorly correlated to soil properties. The choice of using either separate (^{40}K, ^{238}U and ^{232}Th) or combined (dose rate) energy windows, therefore, depends on the patterns established within each energy window (^{40}K, ^{238}U, ^{232}Th). In general, ^{232}Th was the best predictor of soil properties, although dose rate was a better predictor when ^{40}K variability was also present, most likely due to silicate clay translocation.

Stepwise backwards elimination regression indicated that, in general, better predictions of soil texture and calcium carbonate were achieved site-specifically and when ^{40}K, ^{238}U and ^{232}Th were added as separate predictors. As expected, clay, sand, and calcium carbonate models were most heavily weighted by ^{232}Th concentrations, although the latter is weakly influenced by ^{238}U. Analysis of Covariance tests indicated that clay

content and calcium carbonate were more sensitive to changes in site-specific conditions than that of sand content. Regional models for soil property predictions were generally lower in accuracy than its parent-material counterpart.

Proximal and legacy aerial gamma radiometric comparisons within and between sites are in good agreement (except for ^{238}U), with R^2 values as high as 0.92. Dose rate provided the highest amount of agreement between aerial and proximal gamma radiometric measurements, while ^{40}K had the highest amount of agreement with respect to individual energy windows. The finding that aerial ^{40}K was most closely correlated with proximal ^{40}K can be attributed to its high count rate (signal-noise ratio) compared with that of ^{232}Th and ^{238}U.

Spatial misalignment of legacy aerial point data was an issue for several sites, and were subsequently accounted for by considering nearby environmental features such as abrupt changes in geomorphology, forested areas, and large water bodies. The magnitude of shift required was non-systematic within a given survey, and comparisons between aerial and proximal gamma radiometrics after shifting took place were mixed. Explanations for geo-positional inaccuracies stem from the methodology used by the contractors during post-processing.

The work here provides several new insights into the relationship between the field of gamma-ray spectrometry and soil science: 1) calcium carbonate can be mapped with both proximal and aerial gamma radiometrics within a uniform residuum; 2) aerial gamma radiometric spatial patterns general match proximal gamma radiometric spatial patterns when aerial data are properly geo-positioned, 3) thus soil properties can be

mapped by aerial gamma radiometrics through the transitive property; 4) aerial gamma radiometric legacy data in the United States may or may not contain positional errors, and subsequent corrections to these datasets did not necessarily improve proximal gamma radiometrics and aerial gamma radiometric comparisons.

There is still much that needs to be understood about aerial gamma radiometrics for robust implementation as a covariate in soil mapping. This study looked only at four parent materials in areas where aerial gamma radiometrics seemed to have a good correlation with soil properties (Ch. II). Looking at other parent materials such as igneous and metamorphic located across the US would further elucidate the aerial gamma radiometric signal.

CHAPTER IV

SUMMARY

IV.1. Purpose and Outcomes of Study

The overall goal of this project was to gain an understanding regarding aerial gamma-ray spectrometry and its appropriate usage in predicting spatially variable soil properties within the United States. In this study, the following research objectives were therefore posed: 1) identify the usefulness of legacy USDA-NRCS soil property data in explaining aerial gamma radiometric data across the United States; 2) quantify the utility of pre-existing aerial gamma radiometric data in predicting selected soil properties (e.g. clay, sand, CEC, CCE, pH) within both parent material and physiographic types; 3) assess the usefulness of pre-existing aerial gamma radiometric data in comparison with other environmental covariates through predictions of clay content within a given environmental setting; 4) identify relationships between soil properties and gamma-ray spectra using a vehicle-borne gamma-ray spectrometer across different landscapes; and 5) validate aerial gamma-ray spatial patterns with proximal gamma-ray surveys across different landscapes.

IV.2. Assessment of Legacy Aerial Gamma Radiometrics in the U.S.

In Chapter II, objectives 1 through 3 were addressed by analyzing pre-existing aerial gamma radiometric (GR) data against soil samples and their associated soil properties (i.e. texture, CEC, CCE, pH) provided by the United States Department of Agriculture. Initial investigations towards the aerial gamma radiometric data indicated that its

variability could be best understood in terms of physiographic units, followed by parent materials and clay content. Comparisons between the aerial gamma radiometrics and soil properties, therefore, were only conducted after first separating the soil samples into their respective physiographic and parent material types. The locations of these soil samples were found to be unfavorable, as the initial sampling strategy was not designed by the aerial gamma radiometrics feature space.

In general, soil texture and CEC to a lesser extent were most strongly associated with the aerial gamma radiometric response due to a common link in clay mineralogy. As expected the trends between texture and CEC with aerial gamma radiometrics were found to be parent material and region specific. CCE was also significant but more poorly related with aerial gamma radiometric data, while pH was considered unreliable due to poor linearity. Soil properties were most strongly related with aerial gamma radiometrics within flat terrains, whereas relationships within more active geomorphic landscapes such as mountain ranges were poorer most likely due to the influence of erosion. In terms of parent materials, relationships between soil properties and aerial gamma radiometrics were strongest where there were contrasting aerial gamma radiometric responses such as clastic sedimentary parent materials or within coastal or glacial unconsolidated sediments. Finally, the performance of aerial gamma radiometrics in predicting clay content in various landscapes was most successful within unconsolidated sediments within flat terrains, although these results were not necessarily surprising based on the previous analysis.

IV.3. Understanding Aerial Gamma Radiometrics through Proximal Gamma Radiometrics

Chapter III sought to identify the response of aerial gamma radiometrics by conducting surveys closer to the ground, as the latter collects gamma spectra at much higher spatial resolutions. In particular, proximal gamma radiometrics surveys were conducted across various parent materials to determine whether these differently formed soils provided similar responses in terms of aerial gamma radiometrics and soil properties.

Initial results between lab characterized soil texture and CCE measurements with proximal gamma radiometric data indicated that such relationships were stronger than models created through the exploratory analysis from chapter II, suggesting that there is a foundational basis for using proximal gamma radiometrics as surrogate or proxy within field-scales. Relationships between soil properties and proximal gamma radiometrics were found to be site-specific after conducting an Analysis of Covariance Analysis (ANCOVA), meaning that the proximal gamma radiometric response is dependent on parent material type, and this corroborates with the findings from chapter II.

Comparisons between the proximal and aerial measurements were generally significant and high in magnitude (R^2 up to 0.93), although problems were encountered if there was poor spatial positioning from the original survey. Although dose rate comparisons were strongest within the individual sites, aerial and proximal ^{40}K were most strongly correlated across all sites. ANCOVA analysis between proximal and aerial

gamma radiometric models within each site were significantly different in terms of intercept but not slope, suggesting similar responses.

IV.4. Future Directions

This study has shown that aerial gamma radiometrics can become a useful indicator of soil properties such as soil texture if consideration is given towards physiography as well as parent material information. However, there are plenty of knowledge gaps that still remain before such a covariate can become implemented in future digital soil mapping models. For example, legacy aerial gamma radiometric data currently exists within other nations that would benefit from soil information on a national scale such as Brazil and Canada, to name a few. Such analyses are particularly relevant in these areas, as these soils form under different environments and therefore different parent material and physiographic types. As shown in chapter II, any national scale assessments of aerial gamma radiometrics should collect soil samples in such a way that is representative of the parent materials in the area. Additionally, future studies that are concerned with validating aerial gamma radiometric signals either within the U.S. other countries should focus on selecting different landscapes than those chosen for chapter III (for example igneous and/or metamorphic parent materials), as the work was limited to a select amount of parent materials due to time constraints as well as proximity to the Texas A&M campus.

An additional knowledge gap that limits the use of the legacy aerial gamma radiometrics is its quality in terms of appropriate line-spacing distances or distance between adjacent transect lines. In chapter III, the results indicated that aerial gamma

radiometric data was mapping soil properties on the ground due to favorable comparisons between proximal gamma radiometrics and soil properties as well as proximal and aerial gamma radiometric methods, but such correlations were only made in the along-line direction, where the information content was denser. It would, therefore, be interesting to determine if aerial and proximal gamma measurements are comparable across transect lines, as this is a more common occurrence for soils and aerial gamma radiometrics in the United States. Through this type of analysis, it could then be understood if gridded or profile legacy aerial gamma radiometrics are more useful for predicting soil properties across the United States, as the former can potentially average small scale variations in gamma activity.

REFERENCES

Adamchuk, V.I., Hummel, J.W., Morgan, M.T., Upadhyaya, S.K., 2004. On-the-go soil sensors for precision agriculture. Comput. Electron. Agric. 44, 71–91.

Ahl, A., Motschka, K., Slapansky, P., 2014. Precipitation correction of airborne gamma-ray spectrometry data using monitoring profiles: methodology and case study. Explor. Geophys. 45, 8–15.

Annan, A.P., 2002. GPR-history, trends and future developments. Subsurf. Sens. Technol. Appl. 3, 253–270.

Arrouays, D., Grundy, M.G., Hartemink, A.E., Hempel, J.W., Heuvelink, G.B.M., Hong, S.Y., Lagacherie, P., Lelyk, G., McBratney, A.B., McKenzie, N.J., Mendonca-Santos, M.L., Minasny, B., Montanarella, L., Odeh, I.O.A., Sanchez, P.A., Thompson, J.A., Zhang, G., 2014. GlobalSoilMap: Toward a fine-resolution global grid of soil properties, in: Sparks, D. (Ed.), Advances in Agronomy. University of Delaware, Newark, USA, pp. 93–134.

Beamish, D., 2013. Gamma ray attenuation in the soils of northern Ireland, with special reference to peat. J. Environ. Radioact. 115, 13–27.

Beamish, D., 2014. Peat mapping associations of airborne radiometric survey data. Remote Sens. 6, 521–539.

Beamish, D., 2015. Relationships between gamma-ray attenuation and soils in SW England. Geoderma 259-260, 174–186.

Best, M.G., Christiansen, E.H., Deino, A.L., Sherman Gromme, C., McKee, E.H., Noble, D.C., 1989. Excursion 3A: Eocene through Miocene volcanism in the Great Basin of the western United States, in: Chapin, C.E., Zidek, J. (Eds.), New Mexico Bureau of Mines and Mineral Resources. pp. 91–133.

Bierwirth, P., 1996. Investigation of airborne gamma-ray images as a rapid mapping tool for soil and land degradation - Wagga Wagga, NSW. Australian Geological Survey Organisastion, record 1996/22, Canberra.

Billings, S., Hovgaard, J., 1999. Modeling detector response in airborne gamma-ray spectrometry. Geophys. 64, 1378–1392.

Bollhöfer, A., Beraldo, A., Pfitzner, K., Esparon, A., Carr, G., 2013. Pre-mining radiological conditions in the Ranger Project Area. Darwin, Australia.

Boukhenfouf, W., Boucenna, A., 2011. The radioactivity measurements in soils and fertilizers using gamma spectrometry technique. J. Environ. Radioact. 102, 336–339.

Bouma, J., Finke, P.A., 1993. Origin and nature of soil resource variability, in: Robert, P.C., Rust, R.H., Larson, W.E. (Eds.), Soil Specific Crop Management. ASA-CSSA-SSSA, Madison, Wisconsin, pp. 3–14.

Brevik, E.C., Calzolari, C., Miller, B.A., Pereira, P., Kabala, C., Baumgarten, A., Jordán, A., in press. Soil mapping, classification, and pedologic modeling: History and future directions. Geoderma.

Buchanan, S., Triantafilis, J., Odeh, I.O.A., Subansinghe, R., 2012. Digital soil mapping of compositional particle-size fractions using proximal and remotely sensed ancillary data. Geophys. 77, WB201–WB211.

Cardarelli II, J., Thomas, M., Curry, T., Kudarauskas, P., Kappelman, D., Aerial and Ground Radiological Surveys Phosphate Mines in January 2011. Environmental Protection Agency. Erlanger, Kentucky.

Carroll, T., 1981. Airborne soil moisture measurement using natural terrestrial gamma radiation. Soil Sci. 132, 358–366.

Cheney, N., Hempel, J., Odgers, N., McBratney, A.B., Wood, E.F., 2015. dSSURGO: Development and validation of a 30 meter digital soil class product over the 8-million square kilometer contiguous United States, in: EGU General Assembly 2015. Geophysical Research Abstracts 17: EGU2015–11042.

Chervenka, G., 2002. Soil survey of Brazos County, Texas. United States Department of Agriculture in cooperation with Texas Agricultural Experiment Station and Texas State Soil and Water Conservation Board.

Cook, S.E., Corner, R.J., Groves, P.R., Grealish, G.J., 1996. Use of airborne gamma radiometric data for soil mapping. Aust. J. Soil Res. 34, 183–194.

Cresswell, A.J., Sanderson, D.C.W., Harrold, M., Kirley, B., Mitchell, C., Weir, A., 2013. Demonstration of lightweight gamma spectrometry systems in urban environments. J. Environ. Radioact. 124, 22–28.

Darnley, A.G., 1991. The development of airborne gamma-ray spectrometry: case study in technological innovation and acceptance. Nucl. Geophys. 5, 377–402.

Dickson, B.L., Scott, K.M., 1997. Interpretation of aerial gamma-ray surveys - adding the geochemical factors. AGSO J. Aust. Geol. Geophys. 17, 187–200.

Dickson, B.L., 2004. Recent advances in aerial gamma-ray surveying. J. Environ. Radioact. 76, 225–36.

Doolittle, J. a., Brevik, E.C., 2014. The use of electromagnetic induction techniques in soils studies. Geoderma 223-225, 33–45.

Dupont, W.D., Plummer, W.D., 1998. Power and sample size calculations for studies involving linear regression. Control. Clin. Trials 19, 589–601.

Duval, J.S., Carson, J.M., Holman, P.B., Darnley, A.G., 2005. Terrestrial radioactivity and gamma-ray exposure in the United States and Canada, U.S. Geological Survey Open-File Report 2005-1413. Available online only.

English, J.M., Johnston, S.T., 2004. The Laramide orogeny: what were the driving forces? Int. Geol. Rev. 46, 833–838.

Fenneman, N.M., 1917. Physiographic subdivision of the United States. in: Proceedings of the National Academy of Sciences of the United States of America. pp. 17–22.

Ford, K., Harris, J.R., Shives, R., Carson, J., Buckle, J., 2008. Remote predictive mapping 2. gamma-ray spectrometry: a tool for mapping Canada's North. Geosci. Canada 35, 109–126.

Gee, G., Or, D., 2002. Particle-Size analysis, in: Dane, J.H., Topp, G.C. (Eds.), Methods of Soil Analysis: Part 4 Physical Methods, SSSA Book Series 5.4. Soil Science Society of America, Madison, Wisconsin, pp. 255–294.

Gilmore, G.R., 2008. Practical Gamma-ray Spectrometry, 2nd ed. John Wiley & Sons, West Sussex, England.

Geodata International, Inc., 1979, Aerial radiometric and magnetic survey, Austin National Topographic Map, Texas Gulf Coast: U.S. Department of Energy, Open-File Report GJBX-148-79, 2 volumes.

Geometrics, 1980, Aerial gamma ray and magnetic survey, Nebraska/Texas Project, Tyler, Texarkana, and Waco quadrangles of Texas, Oklahoma, Arkansas, and Louisiana: U.S. Department of Energy, Open-File Report GJBX-69-80, 6 volumes.

Gooley, L., Huang, J., Pagé, D., Triantafilis, J., 2014. Digital soil mapping of available water content using proximal and remotely sensed data. Soil Use Manag. 30, 139–151.

Grasty, R.L., Loijens, H.S., Ferguson, H.L., 1973. An experimental gamma-ray spectrometer snow survey over southern Ontario, in: Advanced Concepts and Techniques in the Study of Snow and Ice Resources. pp. 579–593.

Gunn, P.J., Minty, B.R.S., Milligan, P.R., 1997. The airborne gamma-ray spectrometric response over arid Australian terranes, in: Gubins, A.G. (Ed.), Proceedings of Exploration 97: Fourth Decennial International Conference on Mineral Exploration. pp. 733–740.

Hartemink, A.E., Minasny, B., 2014. Towards digital soil morphometrics. Geoderma 230-231, 305–317.

Heinrich, P.V., 2008. Loess map of Louisiana, Louisiana Geological Survey Public Information Series 12. United States Geological Survey. Baton Rouge, Louisiana.

Hendriks, P.H., Limburg, J., de Meijer, R.J., 2001. Full-spectrum analysis of natural gamma-ray spectra. J. Environ. Radioact. 53, 365–80.

Hengl, T., 2007. A Practical guide to geostatistical mapping of environmental variables. EUR 22904 EN. Scientific and Technical Research series. Office for Official Publications of the European Communities, Luxembourg.

Hengl, T., de Jesus, J.M., MacMillan, R.A., Batjes, N.H., Heuvelink, G.B.M., Ribeiro, E., Samuel-Rosa, A., Kempen, B., Leenaars, J.G.B., Walsh, M.G., Gonzalez, M.R., 2014. SoilGrids1km - global soil information based on automated mapping. PLoS One 9, 1–17.

Heuvelink, G.B.M., Webster, R., 2001. Modelling soil variation: Past, present, and future. Geoderma 100, 269–301.

Hill, P.L., Kucks, R.P., Ravat, D., 2009. Aeromagnetic and aeroradiometric data for the conterminous United States and Alaska from the National Uranium Resources Evaluation (NURE) Program of the U.S. Department of Energy: U.S. Geological Survey Open-File Report 2009-1129.

Holliday, V.T., 1989. The Blackwater Draw Formation (Quaternary): a 1.4-plus-m.y. record of eolian sedimentation and soil formation on the Southern High Plains. Geol. Soc. Am. Bull. 101, 1598–1607.

Hovgaard J., Grasty R.L., 1997. Reducing statistical noise in airborne gamma-ray data through spectral component analysis, in: Gubins, A.G. (Ed.), Proceedings of Exploration 97: Fourth Decennial International Conference on Mineral Exploration. pp. 753–760.

IAEA (International Atomic Energy Agency), 2003. Guidelines for radioelement mapping using gamma ray spectrometry data. Vienna, Austria.

IAEA (International Atomic Energy Agency), 2008. Field estimation of soil water content: A practical guide to methods, instrumentation and sensor technology. Vienna, Austria.

Jarvis A., Reuter H.I., Nelson A., Guevara E., 2008. Hole-filled seamless SRTM data V4, International Centre for Tropical Agriculture (CIAT). http://srtm.csi.cgiar.org. Accessed 2 July 2015.

Jenny, H., 1941. Factors of soil formation: a system of quantitative pedology. Dover Publications, New York.

Jurena, M.R., 2005. Soil survey of Burleson County, Texas. United States Department of Agriculture in cooperation with Texas Agricultural Experiment Station and Texas State Soil and Water Conservation Board.

Kayton, M., Fried, W.R., 1997. Avionics Navigation Systems, 2nd ed, Avionics Navigation Systems. John Wiley & Sons, New York, USA.

Kelley, K., 2007. Sample size planning for the coefficient of variation from the accuracy in parameter estimation approach. Behav. Res. Methods 39, 755–766.

Killeen, P.G., 1979. Gamma-ray spectrometric methods in uranium exploration - application and interpretation, in: Hood, P.J. (Ed.), Geophysics and Geochemistry the Search for Metallic Ores. Geological Survey of Canada, Economic Geology report 31, Ottawa, ON, pp. 163–230.

Koch, A., McBratney, A.B., Adams, M., Field, D., Hill, R., Crawford, J., Minasny, B., Lal, R., Abbott, L., O'Donnell, A., Angers, D., Baldock, J., Barbier, E., Binkley, D., Parton, W., Wall, D.H., Bird, M., Bouma, J., Chenu, C., Flora, C.B., Goulding, K., Grunwald, S., Hempel, J., Jastrow, J., Lehmann, J., Lorenz, K., Morgan, C.L., Rice, C.W., Whitehead, D., Young, I., Zimmermann, M., 2013. Soil security: solving the global soil crisis. Glob. Policy 4, 434–441.

Kock, P., Samuelsson, C., 2011. Comparison of airborne and terrestrial gamma spectrometry measurements - evaluation of three areas in southern Sweden. J. Environ. Radioact. 102, 605–613.

Kosanke, K.L., Koch, C.D., 1978. An aerial radiometric data modeling program. IEEE Trans. Nucl. Sci. NS-25, 767–776.

Levi, M.R., Rasmussen, C., 2014. Covariate selection with iterative principal component analysis for predicting physical soil properties. Geoderma 219-220, 46–57.

Loijens, H.S., 1980. Determination of soil water content from terrestrial gamma radiation measurements. Water Resour. Res. 16, 565–573.

Løvberg, L., 1984. The calibration of portable and airborne gamma-ray spectrometers - theory, problems and facilities. Risø Report M-2456. Roskilde, Denmark.

Løvborg, L., Mose, E., 1987. Counting statistics in radioelement assaying with a portable spectrometer. Geophys. 52, 555–563.

Mahmood, H.S., Hoogmoed, W.B., van Henten, E.J., 2013. Proximal gamma-ray spectroscopy to predict soil properties using windows and full-spectrum analysis methods. Sensors 13, 16263–80.

Martelet, G., Drufin, S., Tourliere, B., Saby, N.P.A., Perrin, J., Deparis, J., Prognon, F., Jolivet, C., Ratie, C., Arrouays, D., 2013. Regional regolith parameter prediction using the proxy of airborne gamma ray spectrometry. Vadose Zo. J. 12, 1-14.

Martínez, G., Vanderlinden, K., Giráldez, J.V., Espejo, A.J., Muriel, J.L., 2010. Field-scale soil moisture pattern mapping using electromagnetic induction. Vadose Zo. J. 9, 871-881.

McBratney, A.B., Odeh, I.O.A., Bishop, T.F.A., Dunbar, M.S., Shatar, T.M., 2000. An overview of pedometric techniques for use in soil survey. Geoderma 97, 293–327.

McBratney, A.B., Mendonça-Santos, M.L., Minasny, B., 2003. On digital soil mapping. Geoderma 117, 3–52.

McBratney, A.B., Field, D.J., Koch, A., 2014. The dimensions of soil security. Geoderma 213, 203–213.

McKenzie, N., Ryan, P.J., 1999. Spatial prediction of soil properties using environmental correlation. Geoderma 89, 67–94.

McKenzie, N., Grundy, M., Webster, R., Ringrose-Voase, A., 2008. Guidelines for Surveying Soil and Land Resources, 2nd ed. CSIRO Publishing, Collingwood VIC 3066 Australia.

McRae, S.G., 1972. Glauconite. Earth-Science Rev. 8, 397–440.

Megumi, K., Mamuro, T., 1977. Concentration of uranium series nuclides in soil particles in relation to their size. J. Geophys. Res. 82, 353–356.

Miller, G.B., Greenwade, J.M., 2003. Soil survey of McLennan County, Texas. Soil Survey of McLennan County, Texas. United States Department of Agriculture in cooperation with Texas Agricultural Experiment Station and Texas State Soil and Water Conservation Board.

Minasny, B., McBratney, A.B., 2006. A conditioned Latin hypercube method for sampling in the presence of ancillary information. Comput. Geosci. 32, 1378–1388.

Minty, B.R.S., Luyendyk, A.P.J., Brodie, R.C., 1997a. Calibration and data processing for airborne gamma-ray spectrometry. AGSO J. Aust. Geol. Geophys. 17, 51–62.

Minty, B.R.S., 1997b. Fundamentals of airborne gamma-ray spectrometry. AGSO J. Aust. Geol. Geophys. 17, 39–50.

Minty, Brian, Ross Franklin, Peter Milligan, Murray Richardson, J.W., 2009. The radiometric map of Australia. Explor. Geophys. 40, 325–333.

Moeys, J., 2014. Soiltexture: Functions for soil texture plot, classification and transformation. R package 1.2.19.

Muhs, D.R., Holliday, V.T., 2001. Origin of late Quaternary dune fields on the southern High Plains of Texas and New Mexico. GSA Bull. 113, 75–87.

Nanzyo, M., 2002. Unique properties of volcanic ash soils. Glob. J. Environ. Res. 6, 99–112.

National Cooperative Soil Survey. 2015. National cooperative soil characterization database. Available online at http://ncsslabdatamart.sc.egov.usda.gov. Date accessed: 7/12/2015.

Odgers, N.P., McBratney, A.B., Minasny, B., 2015. Digital soil property mapping and uncertainty estimation using soil class probability rasters. Geoderma 237-238, 190–198.

Petersen, H., Wunderlich, T., Attia al Hagrey, S., Rabbel, W., 2012. Characterization of some Middle European soil textures by gamma-spectrometry. J. Plant Nutr. Soil Sci. 175, 651–660.

Pickup, G., Marks, A., 2000. Identifying large-scale erosion and deposition processes from airborne gamma radiometrics and digital elevation models in a weathered landscape. Earth Surf. Process. Landforms 25, 535–557.

Pitkin, J.A., Duval, J.S., 1980. Design parameters for aerial gamma-ray surveys. Geophys. 45, 1427–1439.

Pracilio, G., Adams, M.L., Smettem, K.R.J., Harper, R.J., 2006. Determination of spatial distribution patterns of clay and plant available potassium contents in surface soils at the farm scale using high resolution gamma ray spectrometry. Plant Soil 282, 67–82.

Priori, R., Bianconi, N., Fantappie, M., Pellegrini, S., Ferrigno, G., Guaitoli, F., Costantini, E.A.C., 2013. The potential of gamma-ray spectroscopy for soil proximal survey in clayey soils. Environ. Qual. 11, 29–38.

Priori, S., Bianconi, N., Costantini, E.A.C., 2014. Can γ-radiometrics predict soil textural data and stoniness in different parent materials? A comparison of two machine-learning methods. Geoderma 226-227, 354–364.

R Development Core Team, 2014. R: A language and environment for statistical computing.

Rachkova, N.G., Shuktomova, I.I., Taskaev, A.I., 2010. The state of natural radionuclides of uranium, radium, and thorium in soils. Eurasian Soil Sci. 43, 651–658.

Rawlins, B.G., Lark, R.M., Webster, R., 2007. Understanding airborne radiometric survey signals across part of eastern England. Earth Surf. Process. Landforms 32, 1503–1515.

Rawlins, B.G., Marchant, B.P., Smyth, D., Scheib, C., Lark, R.M., Jordan, C., 2009. Airborne radiometric survey data and a DTM as covariates for regional scale mapping of soil organic carbon across Northern Ireland. Eur. J. Soil Sci. 60, 44–54.

Rawlins, B.G., Scheib, C., Tyler, A.N., Beamish, D., 2012. Optimal mapping of terrestrial gamma dose rates using geological parent material and aerogeophysical survey data. J. Environ. Monit. 14, 3086–3093.

Reinsch, T., West, L., 2010. The U.S. national cooperative soil characterization database, in: Giles, R., Prakongkep, N. (Eds.), 19th World Congress of Soil Science. IUSS, Brisbane, Australia, pp. 64–67.

Ritchie, J.C., McHenry, J.R., 1990. Application of radioactive fallout cesium-137 for measuring soil erosion and sediment accumulation rates and patterns: A Review. J. Environ. Qual. 19, 215–233.

Rodrigues Jr., F.A., Bramley, R.G.V., Gobbett, D.L., 2015. Proximal soil sensing for Precision Agriculture: Simultaneous use of electromagnetic induction and gamma radiometrics in contrasting soils. Geoderma 243-244, 183–195.

Ryan, P.J., McKenzie, N.J., O'Connell, D., Loughhead, A.N., Leppert, P.M., Jacquier, D., Ashton, L., 2000. Integrating forest soils information across scales: spatial prediction of soil properties under Australian forests. For. Ecol. Manage. 138, 139–157.

Schoeneberger, P.J., Wysocki, D.A., Benham, E.C., Staff, S.S., 2012. Field book for describing and sampling soils, Version 3.0. National Resources Conservation Service, National Soil Survey Center, Lincoln, NE.

Schwarzer, T., Cook, B., Adams, J., 1971. Low altitude gamma-spectrometric surveys from helicopters in Puerto Rico as an example of the remote sensing of thorium, uranium, and potassium in soils and rocks. Remote Sens. Environ. 2, 83–94.

Schwarzer, T.F., Adams, J.A.S., 1973. Rock and soil discrimination by low altitude airborne gamma-ray spectrometry in Payne County, Oklahoma. Econ. Geol. 68, 1297–1312.

Sheather, S.J., 2009. A Modern Approach to Regression with R. Springer, New York.

Sherrod, L.A., Dunn, G., Peterson, G.A., Kolberg, R.L., 2002. Inorganic carbon analysis by modified pressure-calcimeter method. Soil Sci. Soc. Am. J. 66, 299.

Soil Survey Staff, 1993. Soil survey manual. Soil Conservation Service. U.S. Department of Agriculture Handbook 18.

Soil Survey Staff. 1999. Soil taxonomy: A basic system of soil classification for making and interpreting soil surveys. 2nd edition. Natural Resources Conservation Service. U.S. Department of Agriculture Handbook 436.

Soil Survey Staff, 2014. Soil survey field and laboratory methods Manual. Soil Survey Investigations Report No. 51, Version 2.0. R. Burt and Soil Survey Staff (ed.). U.S. Department of Agriculture, Natural Resources Conservation Service.

Soil Survey Staff. Gridded Soil Survey Geographic (gSSURGO) database for the conterminous United States. United States Department of Agriculture, Natural Resources Conservation Service. Available online at http://datagateway.nrcs.usda.gov/. July, 29, 2015a (FY2015 official release).

Soil Survey Staff, Natural Resources Conservation Service, United States Department of Agriculture. Soil Survey Geographic (SSURGO) Database for [Brazos County, Texas]. Available online. Accessed [07/29/2015b].

Soller, D.R., Reheis, M.C., Garrity, C.P., Van Sistine, D.R., 2009. Map database for surficial materials in the conterminous United States: U.S. Geological Survey Data Series 425, scale 1:5,000,000.

Stahr, K., Clemens, G., Schuler, U., Erbe, P., Haering, V., Dinh Cong, N., Bock, M., Dinh Tuan, V., Hagel, H., Le Vinh, B., Rangubpit, W., Surinkum, A., Willer, J., Ingwersen, J., Zarei, M., Herrmann, L., 2013. Beyond the horizons: challenges and prospects for soil science and soil care in Southeast Asia, in: Fröhlich, H.L., Schreinemachers, P., Stahr, K., Clemens, G. (Eds.), Sustainable Land Use and Rural Development in Southeast Asia: Innovations and Policies for Mountainous Areas, Springer Environmental Science and Engineering. Springer Berlin Heidelberg, Berlin, Heidelberg, pp. 31–107.

Stenberg, B., Rossel, R.A.V., Mouazen, A.M., Wetterlind, J., 2010. Visible and near infrared spectroscopy in soil science, in: Sparks, D. (Ed.), Advances in Agronomy. University of Delaware, Newark, USA, pp. 163-215.

Stockmann, U., Malone, B.P., McBratney, A.B., Minasny, B., 2015. Landscape-scale exploratory radiometric mapping using proximal soil sensing. Geoderma 239-240, 115–129.

Taylor, M.J., Smettem, K., Pracilio, G., Verboom, W., 2002. Relationships between soil properties and high-resolution radiometrics, central eastern Wheatbelt, Western Australia. Explor. Geophys. 33, 95–102.

Thompson, J.A., Roecker, S., Grunwald, S., Owens, P.R., 2012. Digital soil mapping: interactions with and applications for Hydropedology, in: Lin, H. (Ed.), Hydropedology. Elsevier, pp. 665–709.

Triplehorn, D.M., 1965. Origin and significance of glauconite in the geologic sequence. Tulsa Geol. Soc. Dig. 33, 282–283.

United States Department of Agriculture, National Resources Conservation Service, 2006. Land resource regions and major land resource areas of the United States, the Caribbean, and the Pacific Basin. U.S. Department of Agriculture Handbook 296.

Viscarra Rossel, R.A., Taylor, H.J., McBratney, A.B., 2007. Multivariate calibration of hyperspectral γ-ray energy spectra for proximal soil sensing. Eur. J. Soil Sci. 58, 343–353.

Viscarra Rossel, R.A., Cattle, S.R., Ortega, A., Fouad, Y., 2009. In situ measurements of soil colour, mineral composition and clay content by vis-NIR spectroscopy. Geoderma 150, 253–266.

Viscarra-Rossel, R.A., Adamchuk, V.I., Sudduth, K.A., McKenzie, N.J., Lobsey, C., 2011. Proximal Soil Sensing: An Effective Approach for Soil Measurements in Space and Time, in: Sparks, D.L. (Ed.), Advances in Agronomy. Elsevier Inc., pp. 237–282.

Viscarra-Rossel, R.A., Webster, R., Kidd, D., 2014. Mapping gamma radiation and its uncertainty from weathering products in a Tasmanian landscape with a proximal sensor and random forest kriging. Earth Surf. Process. Landforms 39, 735–748.

Waters, M.R., Nordt, L.C., 1995. Late Quaternary floodplain history of the Brazos river in east-central Texas. Quat. Res. 43, 311–319.

Wetterlind, J., Tourlière, B., Martelet, G., Deparis, J., P.A. Saby, N., Richer de Forges, A.C., Arrouays, D., 2012. Are there any effects of the agricultural use of chemical fertiliser on elements detected by airborne gamma-spectrometric surveys? Geoderma 173-174, 34–41.

Wilford, J.R., Bierwirth, P.N., Craig, M.A., 1997. Application or airborne gamma-ray spectrometry in soil/regolith mapping and applied geomorphology. J. Aust. Geol. Geophys. 17, 201–216.

Wilford, J., Minty, B., 2006. The use of airborne gamma-ray imagery for mapping soils and understanding landscape processes, in: Lagacherie, P., McBratney, A.B., Voltz, M. (Eds.), Digital Soil Mapping An Introductory Perspective. Developments in Soil Science. Elsevier, Amsterdam, pp. 207–220.

Wilford, J., 2012. A weathering intensity index for the Australian continent using airborne gamma-ray spectrometry and digital terrain analysis. Geoderma 183-184, 124–142.

Wilford, J., de Caritat, P., Bui, E., 2015. Modelling the abundance of soil calcium carbonate across Australia using geochemical survey data and environmental predictors. Geoderma 259-260, 81–92.

Wood, E.F., Roundy, J.K., Troy, T.J., van Beek, L.P.H., Bierkens, M.F.P., Blyth, E., de Roo, A., Döll, P., Ek, M., Famiglietti, J., Gochis, D., van de Giesen, N., Houser, P., Jaffé, P.R., Kollet, S., Lehner, B., Lettenmaier, D.P., Peters-Lidard, C., Sivapalan, M., Sheffield, J., Wade, A., Whitehead, P., 2011. Hyperresolution global land surface modeling: Meeting a grand challenge for monitoring Earth's terrestrial water. Water Resour. Res. 47, W05301.

Wong, M.T.F., Harper, R.J., 1999. Use of on-ground gamma-ray spectrometry to measure plant-available potassium and other topsoil attributes. Aust. J. Soil Res. 37, 267.

APPENDIX A

Division	Province	Section
I. Laurentian Upland (625)	1. Superior Upland (625)	
II. Atlantic Plain (2459)	2. Continental Shelf (not on map)	
	3. Coastal Plain	3a. Embayed section (417)
		3b. Sea Island section (137)
		3c. Floridian section (47)
		3d. East Gulf Coastal Plain (576)
		3e. Mississippi Alluvial Plain (482)
		3f. West Gulf Coastal Plain (800)
III. Appalachian Highlands (2437)	4. Piedmont	4a. Piedmont Upland (430)
		4b. Piedmont Lowlands (113)
	5. Blue Ridge province	5a. Northern section (14)
		5b. Southern section (170)
	6. Valley and Ridge province	6a. Tennessee section (104)
		6b. Middle section (439)
		6c. Hudson Valley (11)
	7. St. Lawrence Valley	7a. Champlain section (79)
		7b. Northern section (14)
	8. Appalachian Plateaus province	8a. Mohawk section (11)
		8b. Catskill section (3)
		8c. Southern New York section (237)
		8d. Allegheny Plateau section (85)

		8e. Kanawha section (411)
		8f. Cumberland Plateau section (80)
		8g. Cumberland Mountain section (11)
		9a. Seaboard Lowland section (75)
		9b. New England Upland section (358)
	9. New England Province	9c. White Mountain section (53)
		9d. Green Mountain section (42)
		9e. Taconic section (36)
	10. Adirondack province	
IV. Interior Plains (11987)	11. Interior Low Plateaus	11a. Highland Rim (606)
		11b. Lexington Plain (11)
		11c. Nashville Basin (11)
	12. Central Lowland	12a. Eastern Lake (1283)
		12b. Western Lake (1941)
		12c. Wisconsin Driftless (408)
		12d. Till Plains (1958)
		12e. Dissected Till Plains (1931)
		12f. Osage Plains (944)
	13. Great Plains	13a. Missouri Plateau (glaciated) (327)
		13b. Missouri Plateau (unglaciated) (640)
		13c. Black Hills (39)
		13d. High Plains (1154)
		13e. Plains Border (363)
		13f. Colorado Piedmont (139)
		13g. Raton (76)
		13h. Pecos Valley (88)
		13i. Edwards Plateau

		13j. Central Texas
V. Interior Highlands (3198)	14. Ozark Plateaus	14a. Springfield-Salem plateaus (3160)
		14b. Boston Mountains (3)
	15. Ouachita province	15a. Arkansas Valley (17)
		15b. Ouachita Mountains (18)
VI. Rocky Mountain System (1308)	16. Southern Rocky Mountains (218)	
	17. Wyoming Basin (164)	
	18. Middle Rocky Mountains (249)	
	19. Northern Rocky Mountains (677)	
VII. Intermontane Plateaus (2628)	20. Columbia Plateau	20a. Walla Walla Plateau (436)
		20b. Blue Mountain section (105)
		20c. Payette section (151)
		20d. Snake River Plain (116)
		20e. Harney section (39)
	21. Colorado Plateaus	21a. High Plateaus of Utah (130)
		21b. Uinta Basin (53)
		21c. Canyon Lands (161)
		21d. Navajo section (121)
		21e. Grand Canyon section (91)
		21f. Datil section (33)
	22. Basin and Range province	22a. Great Basin section (895)
		22b. Sonoran Desert (223)
		22c. Salton Trough (7)
		22d. Mexican Highland (318)
		22e. Sacramento section (35)
VIII. Pacific Mountains	23. Cascade-Sierra Mountains	23a. Northern Cascade Mountains (73)
		23b. Middle Cascade Mountains (171)
		23c. Southern Cascade Mountains (89)

	23d. Sierra Nevada (535)
24. Pacific Border province	24a. Puget Trough (268)
	24b. Olympic Mountains (74)
	24c. Oregon Coast Range (286)
	24d. Klamath Mountains (151)
	24e. California Trough (378)
	24f. California Coast Ranges (481)
	24g. Los Angeles Ranges (98)
25. Lower California province— (24)	

APPENDIX B

Soil sensor voltage measurements were collected two different HH2 Soil Moisture Meters and are subsequently referred to as sensors A and B. For a given sampling site, voltage measurements were collected at the center as well as 1 meter apart from the center for a total of five measurements. Soils were then collected at each of the five sites using a bulk density corer. For more details regarding the procedure, please refer to IAEA (2008).

The samples were located near Texas A&M campus, in particular at the Beef Center or the Animal Sciences Complex, as well the Padina sands located at site B (Caldwell, Texas) within the thesis. Additional data was provided by Diana Bagnall, a previous graduate student from the Hydropedology department at the Texas A&M University Riverside Campus.

Samples were sealed and brought back to the laboratory, where they were then heated to 105 degrees Celsius to determine volumetric water content. Once the oven-dry soil masses were obtained, bulk density values were calculated and finally converted into gravimetric water content using the equation: Gravimetric water content = $\frac{Volumetric\ Water\ Content}{Bulk\ Density}$.

The calibration data, along with the measured voltage readings from the soil samples in Chapter III were imported into R. Predicted gravimetric measurements were then obtained at each site using one of the two calibration equations below, and the

"wet" gamma measurement converted to the "dry" measurement using the following equation adapted from Grasty et al. (1973) and Beamish (2013):

$N_d = \frac{N_w(100 + 1.11 * w)}{100}$, where N_d and N_w are the dry and wet signals; 1.11 is the electron density ratio of water compared with that of soil; and *w* is the gravimetric water content (g g^{-1}). Finally, Pearson correlations were made between soil property and PGR data before and moisture correction and are presented in a table similar manner to that of Priori et al. (2014) below. These results indicate that proximal gamma radiometric corrections for water content need not be applied.

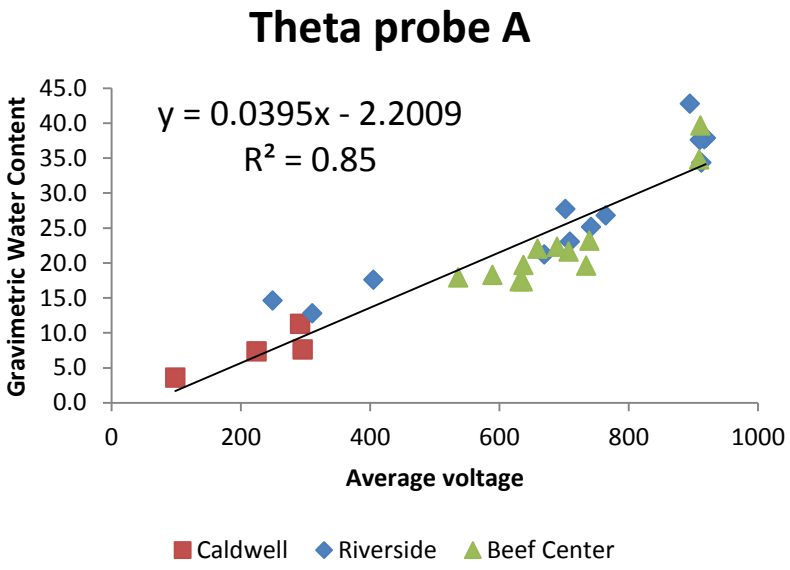

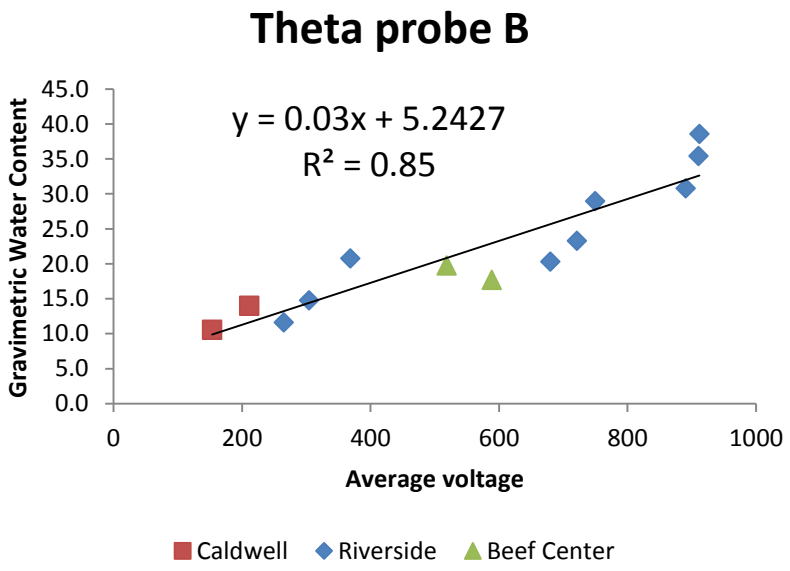

	Total counts		^{40}K		^{238}U		^{232}Th	
	w/o cor.	w/ cor.	w/o cor.	w/ cor.	w/o cor.	w/ cor.	w/o cor.	w/ cor.
Moisture	0.20	0.41	-0.41	-0.40	-0.43	-0.43	-0.43	-0.43
Clay	0.65	0.67	0.33	0.34	0.29	0.29	0.29	0.29
Sand	-0.69	-0.71	-0.33	-0.34	-0.27	-0.27	-0.27	-0.27